DON BOSCO COLLEGE OF ENGINEERING

FATORDA, MARGAO, GOA – 403 602.

DEPARTMENT OF COMPUTER ENGINEERING

2023 – 2024

"Computer Simulation of Neuropathology in Schizophrenia"

By

Mr. Leo Dinar Barros
Mr. Isaiah Abner D'Costa
Mr. Vaughan Royston D'Souza
Mr. Joshua Abel Coutinho
Mr. Duane Francis Rodrigues

Under the Guidance of

Dr. Basabdatta Sen Bhattacharya
Associate Professor,
Brain-inspired Neural Networks Lab,
Department of Computer Science and Information Systems,
BITS Pilani- Goa Campus

Prof. Siya Khandeparkar
Assistant Professor

Dr. Amrita Naik
Assistant Professor

BACHELOR OF ENGINEERING: GOA UNIVERSITY

Certificate

Birla Institute of Technology & Science, Pilani
K K Birla Goa Campus

To whoever it may concern

I hereby certify that the final year students named in the Table below are from the Computer Engineering Dept., Don Bosco College of Engineering, Fatorda, Goa, and have worked under my supervision on their final year project titled 'Computer-based simulation of neuropathology in Schizophrenia'. The work was carried out as a part of ongoing research activities at the Brain-inspired Neural Networks (BINN) Lab, Department of Computer Science and Information Systems, BITS Pilani Goa Campus, during the period September 2023 to April 2024.

Name	Roll No
Leo Barros	2014025
Isaiah D'Costa	2014014
Joshua Coutinho	2014019
Duane Rodrigues	2014007
Vaughan D'Souza	2014062

The work carried out was satisfactory.

Yours sincerely,

BSB

Basabdatta Sen Bhattacharya
Associate Professor, CSIS
D-165 BITS Pilani Goa Campus
NH 17B, Zuarinagar, Sancoale,
Goa 403726, India

Phone: +91 9529266030
lab: https://www.binnlabs-goa.in/the-team

Date: 20-05-2024

ABSTRACT

Schizophrenia, a complex and debilitating mental disorder affecting millions worldwide, poses significant challenges for researchers due to its intricate neural interactions and dynamic cerebral changes. Despite advancements in neuroscience, current research often struggles to capture the multifaceted nature of schizophrenia, limiting the development of effective treatments and interventions. Consequently, there is a pressing need for computational models capable of accurately reproducing the neuropathological characteristics of schizophrenia to deepen our understanding of the disorder. In response to this imperative, The Virtual Brain framework was employed for executing large-scale brain simulations, incorporating the Jansen Rit neural mass model. Drawing on insights from prior studies on neural aberrations associated with schizophrenia, region-specific dysfunction was incorporated into the simulations. The focus centered on modeling functional connectivity, a critical aspect of schizophrenia pathology, through the simulation of Blood Oxygen Level Dependent (BOLD) signals. Leveraging Bayesian optimization techniques, simulation parameters were fine-tuned using empirical data, resulting in a substantial 48% reduction in Mean Squared Error. Furthermore, the study looked to detect the presence of previously identified biomarkers for schizophrenia in the simulation. Through subsequent analysis, the presence of 5 biomarkers was successfully identified, reaffirming the utility of the simulation framework in elucidating key aspects of the disorder.

ACKNOWLEDGEMENT

We extend our sincere gratitude to **Dr. Basabdatta Sen Bhattacharya**, Principal Investigator and Associate Professor, Brain-Inspired Neural Network Lab (BINN), Department of Computer Science and Information Systems, BITS Pilani-Goa Campus for taking us on and guiding us through the fascinating field of computational neuroscience. Apart from domain knowledge, Dr. Bhattacharya imparted valuable research methodologies and practices.

We are also indebted to our Internal Guide **Prof. Siya Khandeparkar** Asst. Professor, Department of Computer Engineering, our co-guide **Prof. Amrita Naik** Asst. Professor, Department of Computer Engineering and reviewer **Prof. Sweta Morajkar** Asst. Professor, Department of Computer Engineering for their timely advice and input.

We would like to thank our Director **Rev. Fr. Kinley D'Cruz** and our principal **Dr. Neena S. P. Panandikar** for providing us with the necessary facilities and the much-needed motivation throughout the project. We are indebted to you. We would like to express our gratitude to our Head of the Department, **Dr. Gaurang Patkar** for showing confidence in us and for giving us timely suggestions and advice with his rich experience and expertise.

TABLE OF CONTENTS

Chapter No.	Contents	Page No.
	Title Page	*i*
	Abstract	
	Acknowledgment	
	Table of Contents	
	List of Figures	
	List of Tables	
1	Introduction	1
2	Literature Survey	4
3	Software Requirement Specification	25
4	Implementation	28
5	Testing and Validation	48
6	Conclusion and Future Scope	50
	References	51

LIST OF FIGURES

Figure No.	Description	Page No.
2.1.1.1	Schematic of the SVM predicting individual diagnostic status and depiction of FSA score calculation.	5
2.1.3.1	(A) Functional MRI measures (DC and VMHC) and Brainnetome 246 atlas. (B) Intensity-based histogram and textural features were extracted from DC and VMHC images. (C) Two-sample t-tests and LASSO were performed for feature selection. (D) An SVM model was built and ROC curve analysis was applied to evaluate model performance.	7
2.1.4.1	Outline of the Striatal Connectivity Index Methodological Approach.	8
2.1.6.1	Overview of ALLF data analysis.	10
2.1.7.1	Schematic overview of the data analysis pipeline.	12
2.1.8.1	3 Major Networks in the Brain.	14
2.1.9.1	ReHo differences between PRS subjects and healthy controls.	16
2.3.2.1	Parcellation atlases.	19
2.3.3.1	fMRI with mask for striatum region.	20
2.3.4.1	fMRI image and Resampled fMRI image in Nilearn.	21
2.3.5.1	fMRI image with 0mm and 5mm smoothing.	22
2.3.5.2	fMRI image with 20mm smoothing.	23
4.1.3.1	Masking data: from 4D Nifti image to 2D data arrays.	29
4.1.3.2	Accuracy v/s train-test slice	30
4.1.3.3	SVM weights plotted on fMRI with mask of striatum	31
4.1.3.4	CNN Architecture	32

Figure No.	Description	Page No.
4.2.3.1	(A) Jansen Rit Model. (B) Diagram of Jansen and Rit model for a cortical column, each color and shape represent one type of column population: pyramidal (blue), excitatory interneuron (green) and inhibitory (red).	35
4.2.7.1	Simulated Functional Connectivity	44
4.2.7.2	Simulated BOLD Time Series	44
4.2.8.1	Simulated Functional Connectivity matrix after optimization	46
4.2.8.2	Simulated BOLD Time Series after optimization	46
5.1	(A) Mean Patient FC. (B) Mean Control FC	47

LIST OF TABLES

Table No.	Description	Page No.
2.3.1	Brain Network and their composite regions	19
4.2.4.1	Configuration of Parameters for the Initial Execution of the Jansen-Rit Model Simulation	41
4.2.4.2	Regions tweaked to show increased or reduced activity based on prior studies reviewed	42
5.1	Test for presence of biomarkers for schizophrenia in the optimized simulation	50

CHAPTER 1:

INTRODUCTION

1.1 Introduction to Project

Schizophrenia, a profound mental disorder, disrupts individuals' thoughts, emotions, and perceptions. Its symptoms range from hallucinations and delusions to disorganized thinking and social withdrawal. This complexity stems from the intricate neural mechanisms underlying the condition.

Computer simulations or modeling provide a compelling opportunity to unravel these complexities. By simulating neural processes, these models aim to replicate the intricate interactions within the brain. Such simulations hold the potential to illuminate the underlying mechanisms of schizophrenia, offering insights into its nature and paving the way for more effective treatment approaches.

1.2 Purpose of the Project

The purpose of this project is to leverage computer simulations to deepen our understanding of schizophrenia. These simulations attempt to replicate brain functions associated with the disorder, providing insights into the neural mechanisms driving its symptoms. In further studies, simulations can potentially serve as a platform to test potential treatments, allowing researchers to simulate the effects of medications or therapies on the modeled brain activity. Additionally, these simulations could facilitate personalized medicine by tailoring interventions based on individual brain patterns observed in the simulations.

1.3 Problem Definition

The project focuses on the development of computational models that simulate intricate neural changes associated with schizophrenia. Specifically, we aim to assess existing research that identifies functional biomarkers indicative of schizophrenia using Machine Learning techniques. Functional Magnetic Resonance Imaging (fMRI) is a neuroimaging technique that measures brain activity by detecting changes in blood flow and oxygenation over a duration of time.

Biomarkers are measurable indicators or characteristics that can be objectively assessed and evaluated as signs of biological processes, conditions, or diseases within the body. In the context of schizophrenia and neuroimaging like fMRI, biomarkers often refer to specific patterns or measurements of brain activity, structure, or function that are associated with the disorder. These biomarkers can include various aspects observed in brain imaging, such as changes in blood flow, neural connectivity, or structural abnormalities that might be indicative of schizophrenia or its progression. We look to validate these studies, and subsequently integrate certain biomarkers into a simulation

model that can faithfully replicate these neural aberrations at the region-level of the brain. Subsequently we also aim to optimize the model on empirical data for better generalizability.

1.4 Existing System

There are several tools available for modeling brain dynamics and understanding neurological conditions:

- **The Virtual Brain**:
  The Virtual Brain [11] is a simulation platform that aims to model and simulate brain dynamics by replicating detailed connectivity patterns which are specific to an individual.

- **NEURON**:
  NEURON [15] is a widely used simulation environment for modeling individual neurons and networks of neurons. While its primary focus is on cellular and subcellular level simulations of neurons and synapses.

- **NEUROLIB:**
  Neurolib [41] is a Python-based computational framework for whole-brain modeling. It offers neural mass models to represent brain region activity on a mesoscopic scale. Researchers can simulate, optimize models, analyze data, and employ evolutionary algorithms for parameter tuning and fitting to empirical data.

- **Brian Simulator:**
  BRIAN [13] is a Python-based open-source simulator for spiking neural networks, offering ease of use for beginners and experts alike.It is highly regarded in the field of computational neuroscience for its ease of use and flexibility, making it suitable for both beginners and experts.

- **NEST:**
  NEST [14] is a simulator focusing on spiking neural network dynamics. Developed by the NEST Initiative, it's ideal for various applications like mammalian visual or auditory cortex processing. NEST offers efficient simulations, synaptic plasticity tools, precise spike timing support, and topological network definition, accessible standalone or via Python (PyNEST).

- **GENESIS:**
  GENESIS [16], (GEneral NEural SImulation System), is a platform supporting a wide range of neural system simulations, from subcellular components to complex single neuron models. Capable of handling large networks and creating system-level models, GENESIS is a comprehensive tool for neural research and study.

These platforms are frameworks for modeling neural dynamics, allowing researchers to simulate various aspects of brain function and connectivity.

1.5 Scope of the project

- **Validate biomarkers**: Create advanced computational models integrating machine learning-identified biomarkers from fMRI scans to simulate schizophrenia-related neural changes.
- **Application of advanced optimization:** Use state of the art of the optimization techniques for the simulation to better mimic empirical brain imaging
- **Integration of user-specified neuroimaging**: The simulation can be optimized on user-provided neuroimaging data to better mimic the empirical data
- **Neural Mechanism Understanding**: The simulation offers insights into the underlying neural mechanisms of schizophrenia, aiding in understanding how specific neural aberrations contribute to the disorder's manifestation.
- **Drug Development and Testing**: By simulating neural responses to potential medications, the model could potentially be used in further studies for predicting drug efficacy and potential side effects, expediting drug development processes.

CHAPTER 2:

LITERATURE SURVEY

2.1 fMRI Biomarkers for schizophrenia

We examined studies that revealed abnormal brain activity patterns linked to schizophrenia. Our search focused on studies that utilized fMRI thereby providing an insight into abnormal functioning in the resting state of a schizophrenia brain. By summarizing these findings, we aimed to identify distinctive dysfunction that could be incorporated into our simulation.

2.1.1 Function Striatal Abnormalities (FSA) Score

The striatum is thought to play a central role in the pathophysiology of schizophrenia. Most individuals with schizophrenia are managed with antipsychotics, all of which essentially rely on the blockade of dopamine D2 receptors in the striatum. In [1], the authors looked to develop a new fMRI biomarker for schizophrenia by quantifying striatal dysfunction as FSA. Participants in this study were recruited from six hospitals in China. The study involved a total of 1,100 subjects, including 560 individuals with schizophrenia and 540 healthy controls, who successfully completed MRI scans after screening. The preprocessing of fMRI data was conducted using the BRANT (Brainnetome Resting-state fMRI Toolkit) version 3.35, a MATLAB toolbox designed for batch preprocessing of fMRI data. The study used the Human Brainnetome Atlas [71] to define and delineate the subregions of the striatum in the human brain.

The study systematically characterized striatal dysfunction using a variety of resting-state fMRI markers, including fractional amplitude of low frequency fluctuations (fALFF) and Regional Homogeneity (ReHo), as well as intra- and extra-striatal functional connectivity (FC). FC provides insights into how different areas of the brain communicate and interact with each other, even when they are not directly connected structurally. ReHo measures the local synchronization of brain activity, reflecting the extent to which the activity in a given region is similar to that of its immediate neighbors. fALFF quantifies the ratio of the amplitude of low-frequency fluctuations (typically in the frequency range of 0.01-0.1 Hz) to the total amplitude across the entire frequency range. The study found that both fALFF and ReHo were significantly increased in the schizophrenia group. These differences were more prominent in the striatum than in other gray matter regions. Additionally, intra-striatal FC was greater between striatal subregions in the schizophrenia group, and extra-striatal FC revealed widespread connectivity differences, particularly in the anterior salience network. These findings indicated substantial alterations in striatal function and its connectivity patterns in individuals with schizophrenia. Having established that FSA (that is, striatal fALFF, intra-striatal FC and extra-striatal FC) provide a robust, reproducible and regionally specific representation of striatal dysfunction in schizophrenia, the researchers aimed next aimed to collapse these

distinct measures of striatal dysfunction into an individualized FSA score, yielding a new biomarker. To this end, they trained Support Vector Machine classifiers to predict the diagnostic status of each individual (schizophrenia versus control group individuals) and defined an individual's FSA score as the shortest distance in the SVM feature space to the separating hyperplane. FSA score polarity was defined such that individuals with positive FSA scores were predicted to belong to the control group. The SVM was trained using the following features: (1) fALFF for each striatal voxel, (2) intra-striatal FC and (3) extra-striatal FC as shown in Fig 2.1.1.1 . However only fALFF was included in the SVM, given that striatal fALFF and ReHo were highly correlated $P < 0.0001$ and that fALFF showed more extensive between-group differences than ReHo.

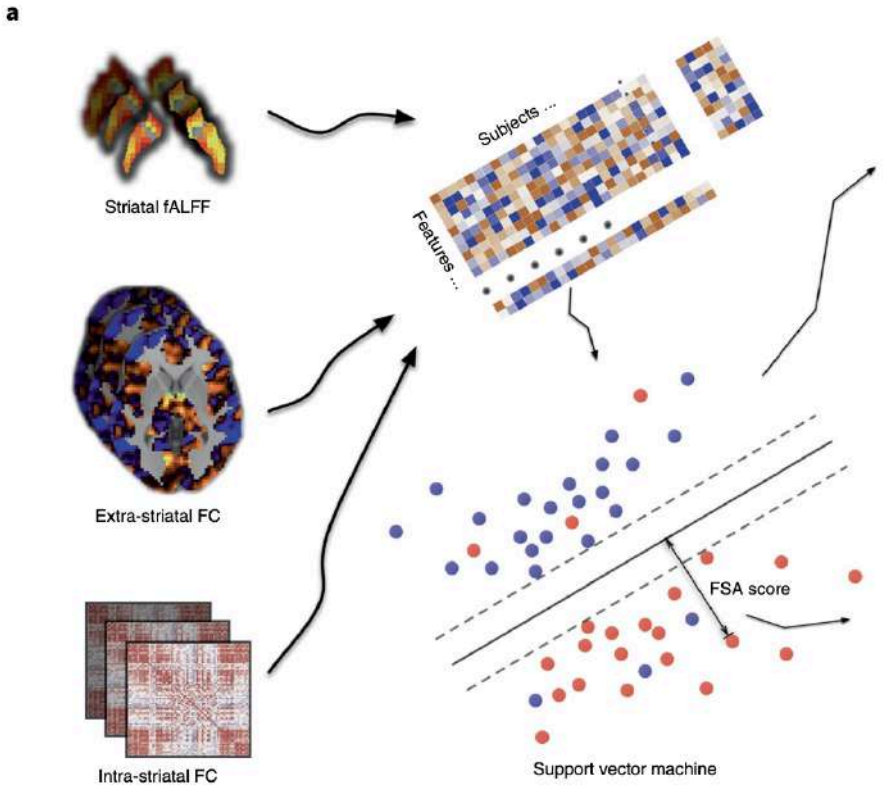

Fig 2.1.1.1: Schematic of the SVM predicting individual diagnostic status and depiction of FSA score calculation. Source: Fig 4.1, A. Li et al 2020 [1]

The feature selection step was omitted to minimize biases and model complexity, and all 12,689 features, including measures of striatal function and FC, were employed in the SVM model. The machine learning library scikit-learn was used for this analysis. A radial basis function kernel was chosen because the feature space was high-dimensional and likely nonlinear. Hyperparameters (C and γ) for the SVM model were optimized through a grid search within the training set. The researchers used an inter-site cross-validation strategy to evaluate the performance of the SVM classifier by training the model using data from six of the seven scanners and testing the model's performance on the data from the remaining scanner. FSA distinguished individuals

with schizophrenia from healthy controls with an accuracy exceeding 80% (sensitivity, 79.3%; specificity, 81.5%).

2.1.2 Reduced Ventral Striatal–Hippocampus Coupling During Reward Processing

Reduced ventral striatal (vST) activation during reward anticipation is an established phenotype in schizophrenia [3], detectable not only in patients but also in unaffected first-degree relatives and correlated with polygenic risk scores (a measure of your disease risk due to your genes) for psychotic disorders. In this study, the researchers investigated the diminished connectivity between the ventral striatum and the hippocampus during reward processing as an endophenotype for schizophrenia. In the context of this study, reward processing refers to the brain's response and neural mechanisms involved in anticipating and experiencing rewards. It involves the activation of specific brain regions, such as the ventral striatum and the hippocampus, during the anticipation and processing of rewarding stimuli. The study aimed to investigate the altered connectivity between the ventral striatum and hippocampus in individuals with schizophrenia and its potential transdiagnostic relevance to mood disorders such as bipolar disorder and major depression. The researchers also explored the association between this altered connectivity and dimensions of psychopathology across disorders. The study included 728 participants, including healthy individuals (n=396), unaffected first-degree relatives, and affected patients with schizophrenia, bipolar disorder, and major depression. Psychiatric diagnoses were confirmed using clinical interviews. The participants underwent fMRI to assess ventral striatal-hippocampus connectivity. The researchers used the Schizotypal Personality Questionnaire to measure psychotic-like experiences and extracted factors related to positive and negative symptoms. They also focused on memory functioning. The results showed that ventral striatal-hippocampus connectivity was altered in schizophrenia, and these alterations extended trans diagnostically to bipolar disorder and major depression. The altered connectivity was associated with positive and negative symptoms and memory dysfunction. The study also examined unaffected first-degree relatives and found that they showed similar alterations in ventral striatal-hippocampus connectivity, suggesting a familial component. Overall, the findings suggest that altered ventral striatal-hippocampus connectivity may be a potential intermediate phenotype across schizophrenia, bipolar disorder, and major depression. It notably aligns with the hypothesis of reduced extra-striatal FC as elucidated in [1].

2.1.3 Degree Centrality and Voxel Mirrored Homotopic Connectivity

This study aimed to identify biomarkers that classify schizophrenia patients and healthy control subjects and investigate the potential neural mechanisms of schizophrenia using degree centrality (DC)- and voxel-mirrored homotopic connectivity (VMHC)-based [4] radiomics. Radiomics involves the extraction and analysis of quantitative features,

including some invisible to the human visual system, from medical images, such as fMRI scans.

The authors conducted a study on patients diagnosed with schizophrenia and Healthy Controls using data from the Center for Biomedical Research Excellence (COBRE) repository hosted on the Neuroimaging Informatics Tools and Resources Collaboratory. Participants underwent structural MRI and resting-state fMRI scans on a 3-T Trio Tim Scanner (Siemens). Data processing, including volume removal, slice timing correction, realignment, segmentation via the new segment approach, image registration through Diffeomorphic Anatomical Registration Through Exponentiated Lie Algebra (DARTEL), spatial normalization via DARTEL (resampling: 3 * 3 * 3 mm^3), removal of nuisance covariates, and bandpass filtering (0.01–0.10 Hz), was performed using Data Processing & Analysis of Brain Imaging and Statistical Parametric Mapping 12. For VMHC, additional steps included registering pre-processed images to a symmetric template and smoothing with a Gaussian kernel. Fisher's z-transformations were applied to the resulting DC and VMHC maps.

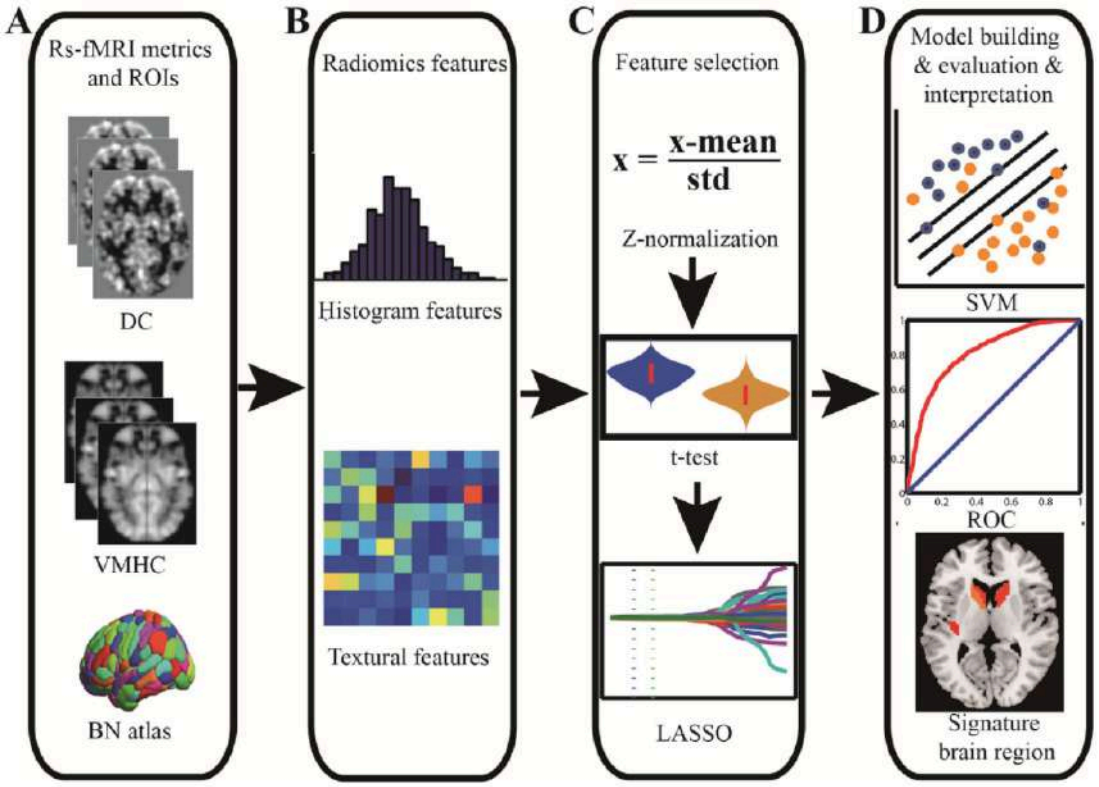

Fig 2.1.3.1: (A) fMRI measures (DC and VMHC) and Brainnetome 246 atlas. (B) Intensity-based histogram and textural features were extracted from DC and VMHC images. (C) Two-sample t-tests and LASSO were performed for feature selection. (D) An SVM model was built and ROC curve analysis was applied to evaluate model performance. Source: Fig 1, D. Shi et al. 2022 [4]

In-house scripts were employed for feature extraction, using the Brainnetome 246 atlas to obtain 15 intensity-based histograms and 33 texture features from individual DC and VMHC maps, resulting in a total of 23,616 features [(15 + 33) * 246 * 2 = 23,616] for

each participant. Feature selection involved t-tests and Least Absolute Shrinkage and Selection Operator (LASSO) to reduce dimensionality. LASSO regression prevents overfitting in linear models by constraining coefficient values, reducing errors, and enhancing accuracy. Nested ten-fold cross-validation was utilized for model evaluation and hyperparameter tuning (optimal λ of LASSO) in a SVM classifier. Standardization of features to z-scores preceded the process. The SVM classifier (linear kernel, C = 1) determined the state (Schizophrenia patient or Healthy Control) through ten-fold cross-validation (repeated 20 times). Performance metrics included mean accuracy, balanced accuracy, AUC, F1 score, sensitivity, specificity, and precision. ROC curve analysis assessed model performance, with permutation tests confirming classification significance (AUC and accuracy). The SVM model with a linear kernel provided feature weights, where positive weights indicated higher measurement in schizophrenia patients, negative weights indicated higher measurement in healthy controls, and the absolute value represented the feature's contribution to classification. The optimal λ of LASSO was tuned using grid search based on classification accuracy, resulting in an AUC of 0.808 and accuracy of 74.02%.

2.1.4 Striatal Connectivity Index (SCI)

In the search for prognostic biomarkers in schizophrenia, particularly to predict clinical response to antipsychotic drugs, recent research [2] has spotlighted the potential of resting state fMRI. Their research indicates that intrinsic connectivity patterns of the striatum could serve as a predictive biomarker for treatment outcomes in schizophrenia.

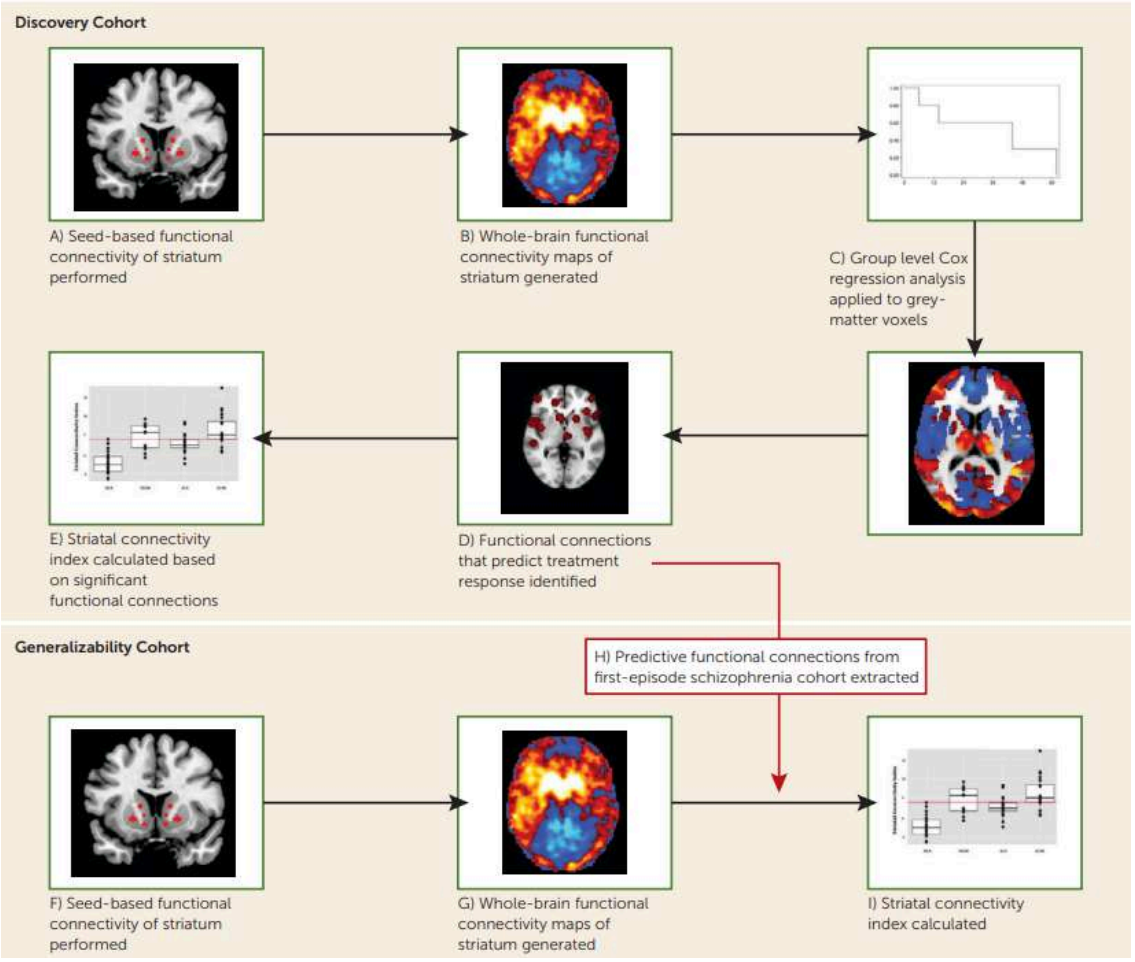

Fig 2.1.4.1: Outline of the Striatal Connectivity Index Methodological Approach Source: Fig 1, Sarpal et al. 2016 [2]

Initially, the study focused on a discovery cohort of 41 first-episode schizophrenia patients. At the outset of their treatment with second-generation antipsychotics, each patient underwent resting-state fMRI scanning to capture FC maps. These maps were derived from striatal seed regions, reflecting the complex neural interplay within the brain. Through the use of survival analysis and Cox regression applied to the connectivity data, researchers identified 91 regions functionally connected to the striatum that provided significant prognostic information. These connections formed the basis of the SCI, a predictive model for assessing the likelihood of a positive clinical response to antipsychotic medication. The robustness of this model was not only demonstrated in the discovery cohort but also in an independent generalizability cohort comprising 40 newly hospitalized chronic schizophrenia patients with acute psychosis.

The results were telling: the SCI predicted antipsychotic treatment response with high sensitivity and specificity in both cohorts. This finding is pivotal, underscoring the index's potential to differentiate between likely responders and non-responders to treatment .The positive predictive value of 76% and a negative predictive value of 79%, further attest to the index's clinical applicability.

2.1.5 Resting State Cortical Connectivity

Parallel to the study on striatal connectivity, the investigation in [5] focused on the superior temporal cortex, a critical region for auditory processing and sensory integration. By analyzing the baseline functional connections of this region to other cortical areas, the study found that the strength and characteristics of these connectivity patterns could predict clinical response to antipsychotic medications with a balanced accuracy of 82% . This high degree of accuracy was achieved through the application of machine learning algorithms to FC data, suggesting that resting-state cortical connectivity could be a robust predictor of both positive and negative treatment responses.

The study on resting state cortical connectivity in first-episode drug-naive (FEDN) schizophrenia patients employed a comprehensive approach, encompassing participant selection, treatment, symptom assessment, MRI data acquisition, and advanced statistical analyses. The study's statistical analyses were centered around the comparison of FC between FEDN schizophrenia patients and healthy control. This involved calculating the mutual information and zero-lag correlation between regional time series of BOLD signals, and performing t-tests to assess group differences. The false discovery rate was controlled to maintain statistical rigor. Furthermore, machine learning techniques, specifically SVM, were employed to classify patients and predict treatment response, using FC features derived from the MRI data. This comprehensive methodology enabled the exploration of the differences in brain connectivity patterns between FEDN schizophrenia patients and healthy individuals, offering insights into the potential predictive markers of treatment response in schizophrenia

The study successfully identified FEDN schizophrenia patients with an accuracy of 78.6% and predicted their responses to antipsychotic treatment with an accuracy of 82.5% at an individual level.

2.1.6 Amplitude of Low-Frequency Fluctuation (ALFF)

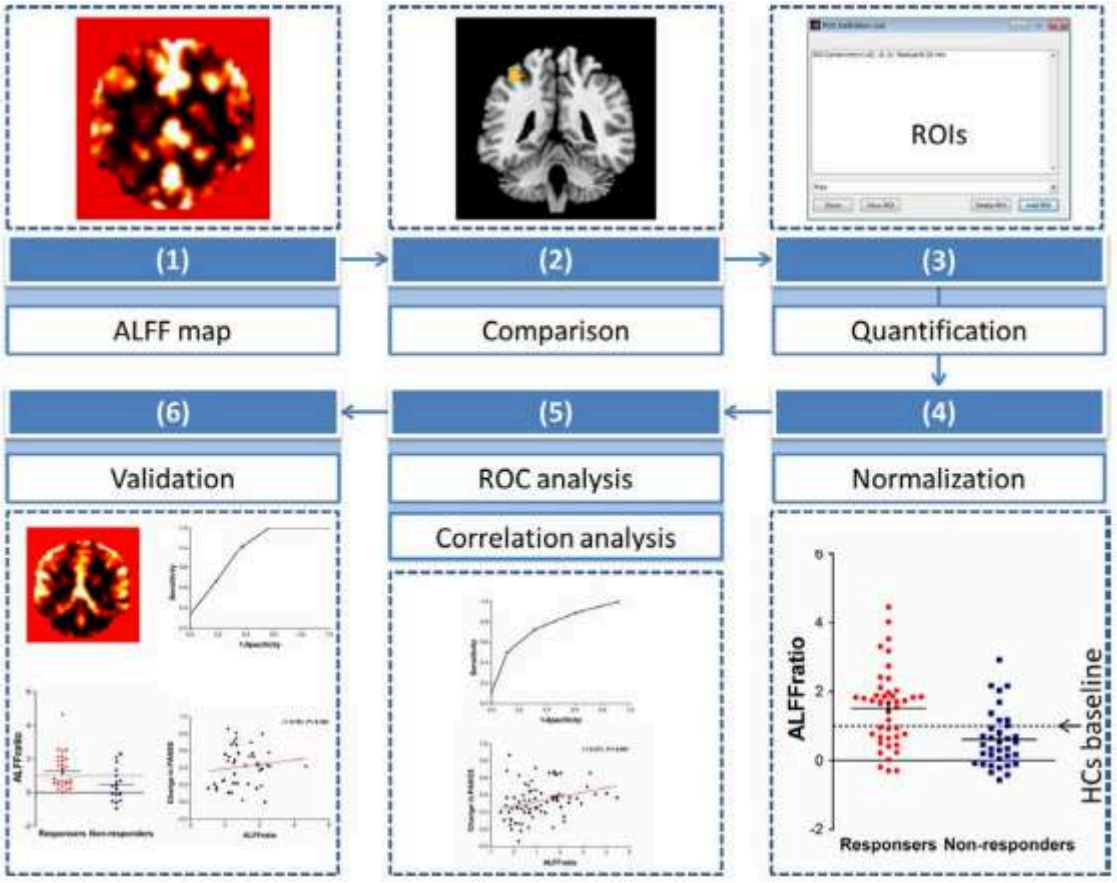

Fig 2.1.6.1: Overview of ALLF data analysis. Source: Fig 1, Cui et al. 2019 [6]

In the ongoing quest to find biomarkers that can predict the treatment response in schizophrenia, the study conducted by Long-Biao Cui, Min Cai, Xing-Rui Wang, and colleagues [6] stands out as a vital contribution. The team's research aimed to identify and validate a neuroimaging signature, specifically the amplitude of low-frequency fluctuation (ALFF), that could indicate early response to treatment in patients with schizophrenia. The study involved 100 patients with schizophrenia from the Department of Psychiatry at Xijing Hospital and 92 healthy controls. ALFF maps were computed for each participant to capture baseline brain activity, followed by a voxel-based comparison to distinguish regions where ALFF values differentiated between treatment responders and non-responders. This led to the extraction of ALFF values from specific regions of interest, identified based on peak coordinates in clusters that varied between the two groups. Further enhancing the analysis, these patient-specific ALFF values were normalized against the mean ALFF values of healthy controls, creating an ALFF ratio that facilitated a normative comparison.

The effectiveness of the ALFF ratio as a predictive marker was rigorously evaluated through receiver operating characteristic (ROC) analysis, correlating it with clinical scales, the length of hospital stay, and antipsychotic dosage. The robustness of this methodology is highlighted by the area under the ROC curve for the baseline ALFF

ratio, recorded at 0.746. This value indicates the ALFF ratio's moderate accuracy in distinguishing between treatment responders and non-responders, underscoring its potential utility as a biomarker in clinical practice for schizophrenia treatment outcomes.

The sensitivity, specificity, and accuracy were calculated to be 72.7%, 68.6%, and 70.9%, respectively, in the primary dataset. These performance metrics were validated in an independent replication dataset, strengthening the reliability of the ALFF ratio as a biomarker. The consistency of results across both the principal and replication datasets attests to the potential of baseline brain activity, as gauged by fMRI, to serve as a predictive marker for early treatment response in schizophrenia.

2.1.7 Gray Matter Volume (GMV), fALFF, ReHo

The study [7] focuses on Deficit schizophrenia, characterized by enduring negative symptoms, and stands out as a promising and distinct subtype within the heterogeneous landscape of schizophrenia. Distinguishing deficit schizophrenia from non-deficit schizophrenia has been a subject of increasing interest, driven by the recognition of differential etiopathophysiology, prevalence, and clinical outcomes associated with these subtypes. In this context, the study delved into the neural underpinnings of deficit syndrome, leveraging a multimodal neuroimaging approach. Through the integration of fMRI and structural MRI, the aim is to identify biomarkers capable of discriminating deficit schizophrenia from non-deficit schizophrenia and healthy controls. Key neuroimaging features, including GMV, fALFF, and ReHo, are extracted to comprehensively characterize deficit schizophrenia. Employing machine learning, specifically SVM classification models, this research seeked to enhance the understanding of the specific neurobiological signatures associated with deficit schizophrenia, offering valuable insights for improved clinical assessment and intervention strategies.

A total of 183 male participants diagnosed with schizophrenia were recruited from Yangzhou Wutaishan Hospital in Jiangsu Province, China. Inclusion criteria required a confirmed Diagnostic and Statistical Manual of Mental Disorders, Fourth Edition (DSM-IV) diagnosis, and deficit schizophrenia was diagnosed using the Chinese version of Schedule for the Deficit Syndrome (SDS). Non-deficit schizophrenia participants were those not meeting SDS criteria, while healthy control subjects were matched for age, gender, and education. Clinical measurements utilized the Brief Psychiatric Rating Scale and the Scale for the Assessment of Negative Symptoms. Brief Psychiatric Rating Scale covered positive, negative, disorganized, and affect syndromes, while Scale for the Assessment of Negative Symptoms focused on negative symptoms, categorized into motivation and pleasure and diminished expressivity. MRI data were acquired with a 3.0T MRI scanner, involving both structural MRI and fMRI during resting-state sessions at Subei Hospital, Yangzhou. The imaging processing pipeline involved preprocessing of fMRI data using Statistical Parametric Mapping 12

and Data Processing and Analysis for Brain Imaging toolkit. Nuisance signals were regressed out during preprocessing.

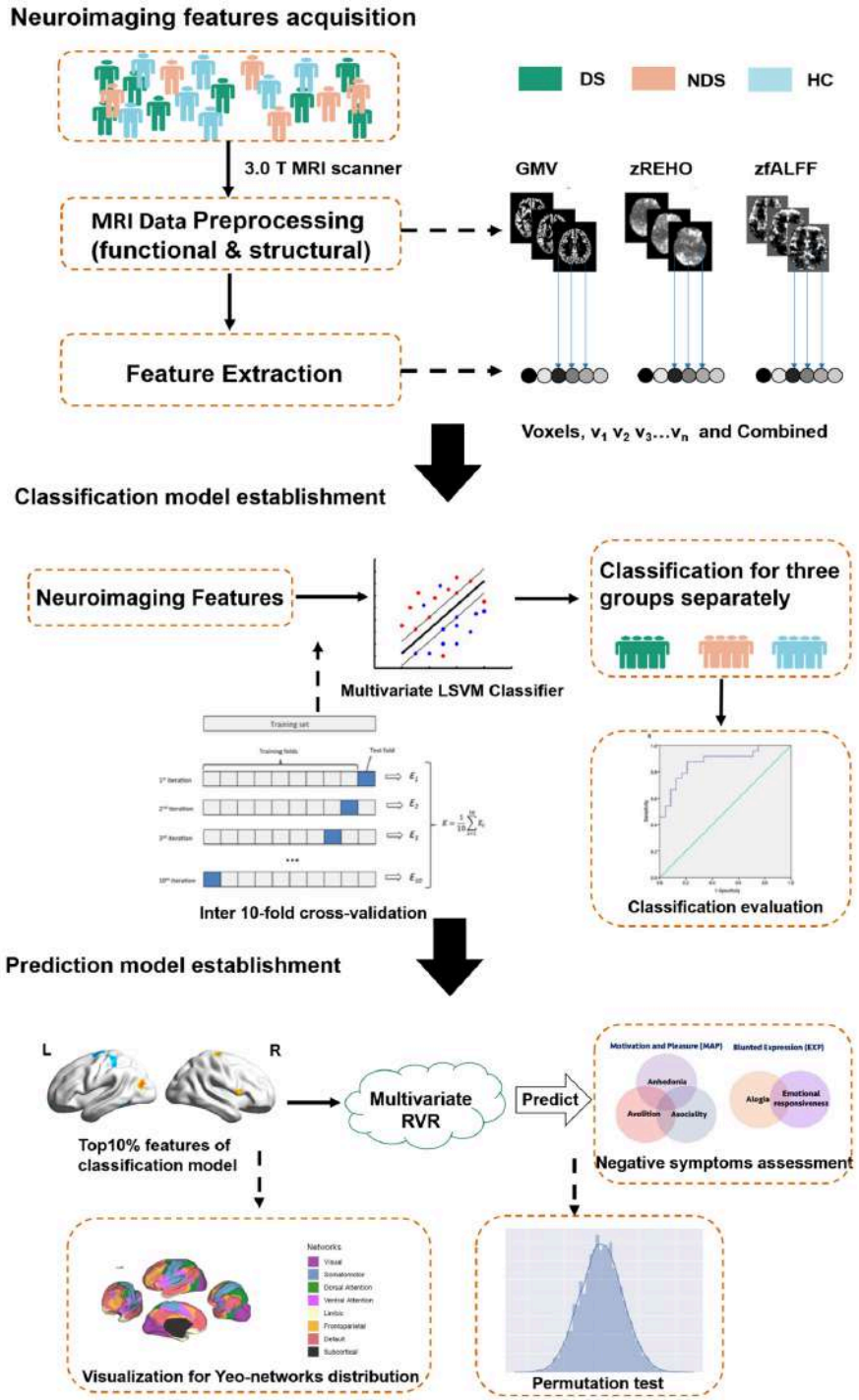

Fig 2.1.7.1: Schematic overview of the data analysis pipeline. Source: Fig 1, Gao et al. 2023 [7]

As can be seen in Fig 2.1.7.1, model features, including GMV, fALFF, and ReHo, were computed post-preprocessing. GMV was indicative of structural brain information, fALFF examined low-frequency fluctuations, and ReHo measured the complexity of brain function. The methodology employed statistical techniques to analyze

biomarker-clinical measure relationships. Subgroup analyses were conducted for participant variations, enhancing findings' robustness. The study prioritized a detailed examination of the identified biomarker's implications for schizophrenia.

The study encompassed a comprehensive exploration of deficit schizophrenia and non-deficit schizophrenia through multimodal neuroimaging analyses. Notably, the multimodal classifier exhibited heightened accuracy (75.48%) compared to single-modal models in distinguishing deficit schizophrenia from non-deficit schizophrenia. The discriminative features, extracted from GMV, fALFF, and ReHo, revealed distinct patterns across brain regions. GMV abnormalities were prominent in the bilateral inferior frontal gyrus orbital part, superior temporal gyrus, precentral gyrus, and other regions, with a spatial emphasis on visual, default mode, somatomotor, and dorsal attention networks. Functional features, including fALFF and ReHo, displayed abnormalities in areas such as the superior occipital gyrus, inferior temporal gyrus, superior frontal gyrus orbital part, lingual gyrus, and cingulate gyrus. Strikingly, the identified discriminative features significantly predicted scores of the diminished expressivity factor in deficit schizophrenia but not in non-deficit schizophrenia. Moreover, the relevance vector regression analysis demonstrated a positive association between predicted and actual scores in the diminished expressivity factor of deficit schizophrenia, shedding light on the predictive value of these neuroimaging features for specific negative symptom subdomains.

2.1.8 Functional Networks

The study outlined in [8] looked to assess functional networks in the brain as a classification feature for schizophrenia. The study included 60 schizophrenia patients, 43 unaffected first degree relatives of patients (18 siblings, 15 sons/daughters, and 10 parents), and 50 Healthy Controls. Of the 43 unaffected first degree relatives, 10 were relatives of the patients recruited in this study. An independent dataset of 40 patients and 40 controls was used as a validation to evaluate the performance of classifiers.

MR images were collected using a Siemens Magnetom Trio 3.0 Tesla imaging system with a standard head coil at Peking University Third Hospital. For image registration, high-resolution structural T1 MRI data were acquired . Resting state fMRI scans were obtained using a gradient-recalled echo-planar imaging sequence. The final sample comprised 40 controls, 34 first degree relatives, and 42 schizophrenia patients.

A pattern classification method was used to identify informative functional networks and build SVM classifiers to distinguish 32 patients from 30 controls. The pattern classifiers were built on a subset of functional networks that were selected to optimize the classification performance for distinguishing schizophrenia patients from Healthy Controls using an SVM classification algorithm. The SVM classification was based on similarity measures between subjects computed based on their functional networks. Classifiers were first built on individual function networks, one for each functional network, then the classifiers were evaluated with a leave-one-out cross-validation, and

evaluated using the same cross-validation.The best combination of Functional networks with the overall best classification performance was to be included in the final classification.

The informative functional networks included the default mode network, cerebellum, ventral frontotemporal network, and posterior default mode network with parahippocampal gyrus. The accuracy of the classifiers built upon the informative functional networks was 83.9% sensitivity 87.5%, specificity 80% with an AUC of 0.914. The classification results on an independent testing dataset showed that the identified informative functional networks achieved good performance with a correct classification rate of 77.5% and AUC of 0.811.

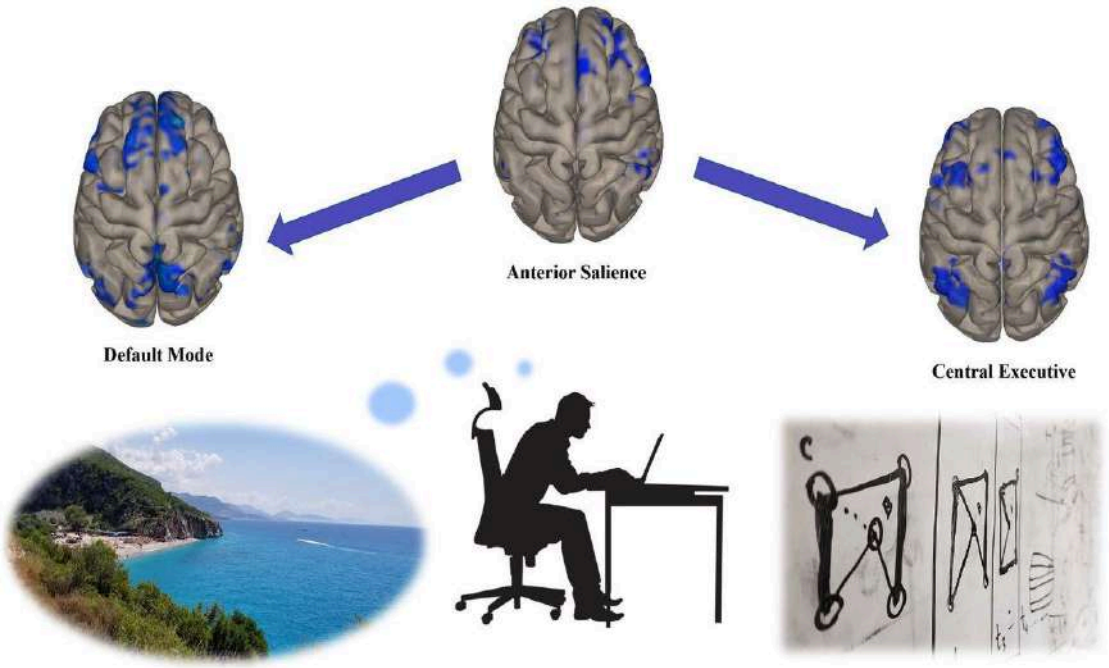

Fig 2.1.8.1: 3 Major Networks in the brain Source: Fig 3, Chengping Rao, 2020 [60]

In conclusion, large-scale functional networks identified by a pattern classification method were informative for quantifying structural alteration in the brain as well in schizophrenia as well as in first degree relatives. The classification scores of the first degree relatives and schizophrenia patients were correlated with their digit symbol coding scores. These findings suggest that pattern recognition of large-scale Functional networks could be used as a biomarker for unaffected first degree relatives with schizophrenia-specific FC patterns, and may help early recognize and treat individuals at high risk of schizophrenia [9]. The informative functional networks included default mode network, cerebellum, ventral frontal temporal network, and p-default mode network were largely consistent with previous findings. FC and multimodal neuroimaging studies revealed that schizophrenia variably involves several altered brain regions and circuits [10], and family members of schizophrenia patients might share similar changes.

2.1.9 ReHo

The study investigates ReHo patterns in individuals presumed to be at risk for a specific condition (PRS) compared to healthy controls [28]. Resting state fMRI data were analyzed using the REST software. Significant ReHo alterations were observed in specific brain regions among PRS subjects, providing potential neurobiological markers for discriminating them from healthy controls. Correlation analyses explored associations between ReHo values and clinical characteristics in PRS subjects. Additionally, discriminative potential was assessed through Receiver Operating Characteristic (ROC) and SVM analysis. Identified brain regions with significantly different ReHo values underwent receiver operating characteristic analysis to assess their potential as markers for discriminating PRS subjects from controls. Finally, a classification analysis using SVM with parameter optimization and leave-one-out Cross-validation was employed to evaluate the discriminatory power of ReHo clusters between PRS subjects and controls.

ReHo Group Differences: PRS subjects exhibited significant ReHo decreases in the left inferior temporal gyrus, and increases in the right inferior frontal gyrus and right putamen compared to controls. Correlations between ReHo Values and Clinical Characteristics in PRS Subjects: ReHo values in the left inferior temporal gyrus positively correlated with disorganized symptoms, and those in the right putamen negatively correlated with general symptoms, though these correlations were not significant after Bonferroni correction.

Discriminating PRS Subjects from Controls: The left inferior temporal gyrus showed potential as a discriminating marker with an area under the curve of 0.800, sensitivity of 91.89%, and specificity of 58.82%. The right inferior frontal gyrus and right putamen also exhibited discriminatory potential. SVM analyses revealed combinations of ReHo values providing optimal sensitivity, specificity, and accuracy, with the combination of values in all three brain regions achieving a sensitivity of 88.24%, specificity of 91.89%, and accuracy of 90.14%.

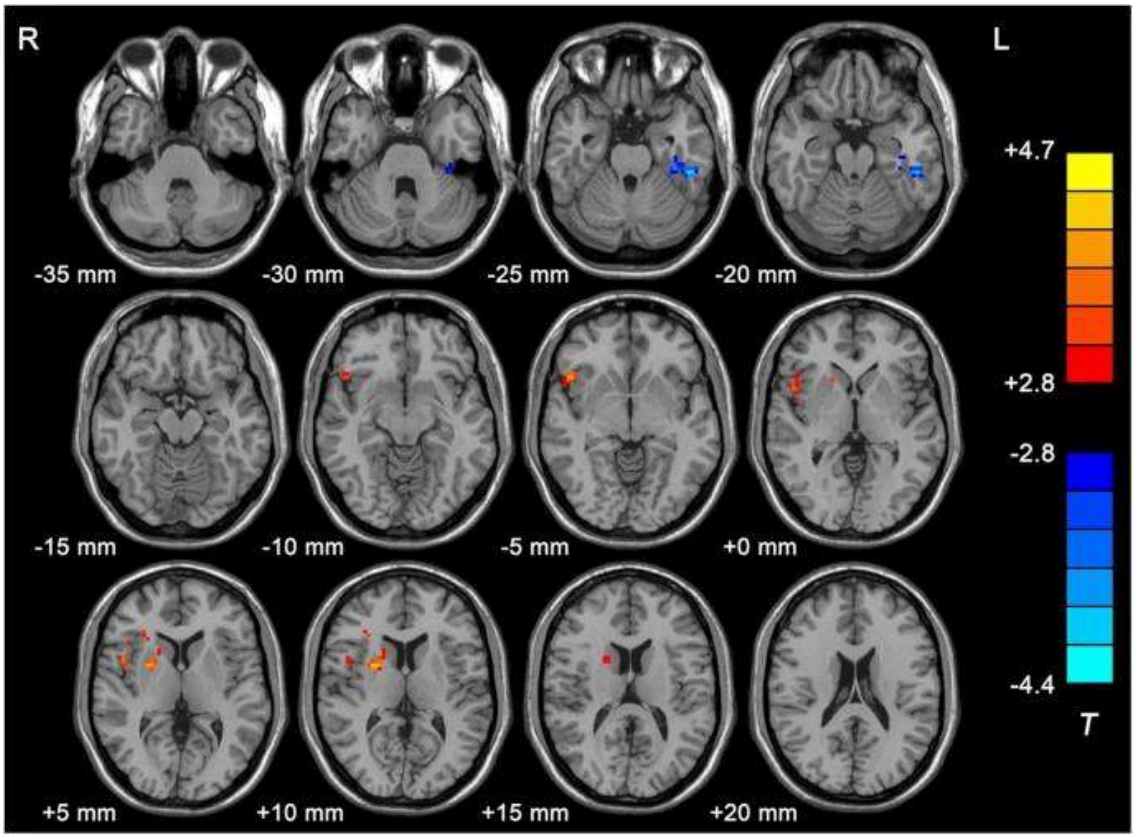

Fig 2.1.9.1: ReHo differences between PRS subjects and healthy controls. Source: Fig 1, Y. Zhang, L. Lv, et al 2016 [28]

2.2 Regions exhibiting dysfunction in Schizophrenia

To mimic region-level perturbations in the simulation model, a literature survey was conducted to provide insight into regions that exhibited abnormally high or abnormally low activity in the fMRI of schizophrenia patients.

In [29], alterations in FC patterns were evident across various brain networks in individuals with schizophrenia. Specifically, regions within the visual network, sensorimotor network, dorsal attention network, ventral attention network, and thalamus exhibited notable increases, while FC variability in brain regions spanning the default mode network and frontal-parietal network to the entire brain displayed significant decreases. Additionally, [30] highlighted diminished FC between the bilateral hippocampi and areas implicated in episodic memory, including the posterior cingulate cortex, extrastriate cortex, medial prefrontal cortex, and parahippocampal gyrus, in schizophrenia patients. Furthermore, [37] unveiled disrupted FC linked to the anterior insula's modulation of large-scale brain networks in schizophrenia. Alterations were observed in the right anterior insula's modulation of the central executive and default mode networks, potentially contributing to the cognitive deficits seen in individuals with schizophrenia. Moreover, [38] demonstrated considerable reductions in FC strength at the regional level within various cortical regions, such as the medial premotor, cingulate, and parietal cortex, precentral and postcentral cortex, occipital

association cortex, and left inferior frontal, superior temporal, and insular cortex in schizophrenia patients. Lastly, [39] revealed lower gray matter density compared to controls in a network of regions, including the bilateral insular cortex, anterior cingulate gyrus, left parahippocampal gyrus, middle frontal gyrus, postcentral gyrus, and the thalamus. These abnormalities were shown to progress from the first episode to the chronic stage of schizophrenia.

2.3 Abnormalities observed in FC of schizophrenia

The study [65] can be used to note that aberrant intrinsic FC within the Salience Network's right anterior insula by affecting interactions between the default mode network (default mode network) and Central Executive Network, showing increased FC between these networks potentially influencing self-referential and goal-directed cognitive processes. The study [66] suggests that schizophrenia is associated with deficits in both within-network and between-network connectivity of the frontoparietal network, a key network involved in executive control. Specifically, individuals with schizophrenia exhibited cortico-subcortical disconnections within the frontoparietal network, alongside increased FC between the sensory processing and the default mode network.

As specified in [67], the default mode network consisted of various abnormalities in schizophrenia patients. It showed increased activity in the default mode network- a result of a process of massive reassociation of traces in schizophrenia, potentially aimed at minimizing excess free energy in psychosis. By integrating neuroimaging data with Freudian theory, the study sheds light on the underlying mechanisms of schizophrenia, emphasizing the significance of default mode network hyperactivity in the psychopathology of the disorder. The study [70] revealed alterations in FC involving the cerebellum in schizophrenia patients. An increase in FC between the cerebellum, and the prefrontal cortex, indicating potential disruptions in cognitive and executive functions was found. Conversely, a decrease in FC between the cerebellum and the visual cortex, suggesting impaired integration of sensory information. Besides this, reduced FC was observed between the cerebellum and the sensorimotor cortex, implying disturbances in motor coordination and sensory processing. Table 2.3.1 encompasses the composite regions within Connectivity-96 that make up key networks within the brain.

Brain Network	**Composite regions present in Connectivity-96**
Visual network	Anterior visual area, ventral part Visual area 2 (secondary visual cortex) Anterior visual area, dorsal part Visual area 1 (primary visual cortex)
Sensorimotor network	Secondary somatosensory cortex Primary somatosensory cortex Ventrolateral premotor cortex Primary motor cortex Dorsolateral premotor cortex
Dorsal attention network	Frontal eye field
Default mode network	Dorsomedial prefrontal cortex
Frontal–parietal network	Anterior insula Anterior cingulate cortex Ventrolateral prefrontal cortex Dorsolateral prefrontal cortex Inferior parietal cortex Medial parietal cortex Intraparietal cortex Superior parietal cortex

Table 2.3.1: Brain Networks and their composite regions

2.4 Processing of fMRI

2.4.1 Preprocessing of raw fMRI

Preprocessing of fMRI involves reducing noise from physiological factors and motion artifacts, aligning data spatially and temporally, normalizing intensity, and applying spatial smoothing. Detrending removes systematic trends, while normalization ensures data comparability across scans and sessions. Corrections for slice timing and filtering focus on specific frequency bands of interest. Artifact removal targets spikes or outliers, and masking isolates a region of interest. Brain extraction removes non-brain tissues, and the overall result is a refined dataset that improves the accuracy of studying brain function and connectivity. For the purpose of our study, we chose to use pre-processed fMRI datasets owing to the complexity and domain-specific nature of the work.

2.4.2 Parcellation

In the field of neuroimaging, particularly in methods like MRI and fMRI, the brain is often analyzed by dividing it into distinct regions through a process known as parcellation. Parcellation is essential for understanding the organization and function of different brain areas and for analyzing neuroimaging data effectively. One common approach to parcellation involves the use of brain atlases, which are reference maps delineating the brain's anatomical or functional regions based on various criteria such as cytoarchitecture, connectivity patterns, or functional properties. These atlases serve multiple purposes in neuroimaging research and clinical practice. Firstly, they provide a standardized anatomical reference, allowing researchers and clinicians to precisely identify and label different brain regions for consistent communication and comparison across studies. Secondly, atlases enable researchers to define specific regions of interest within the brain for further analysis, facilitating the study of brain activity or connectivity in relation to specific tasks or conditions. Commonly used brain atlases include the Talairach, Harvard-Oxford, AAL, Desikan-Killiany, and Brodmann areas, each providing standardized references for anatomical localization or functional regions in neuroimaging research.

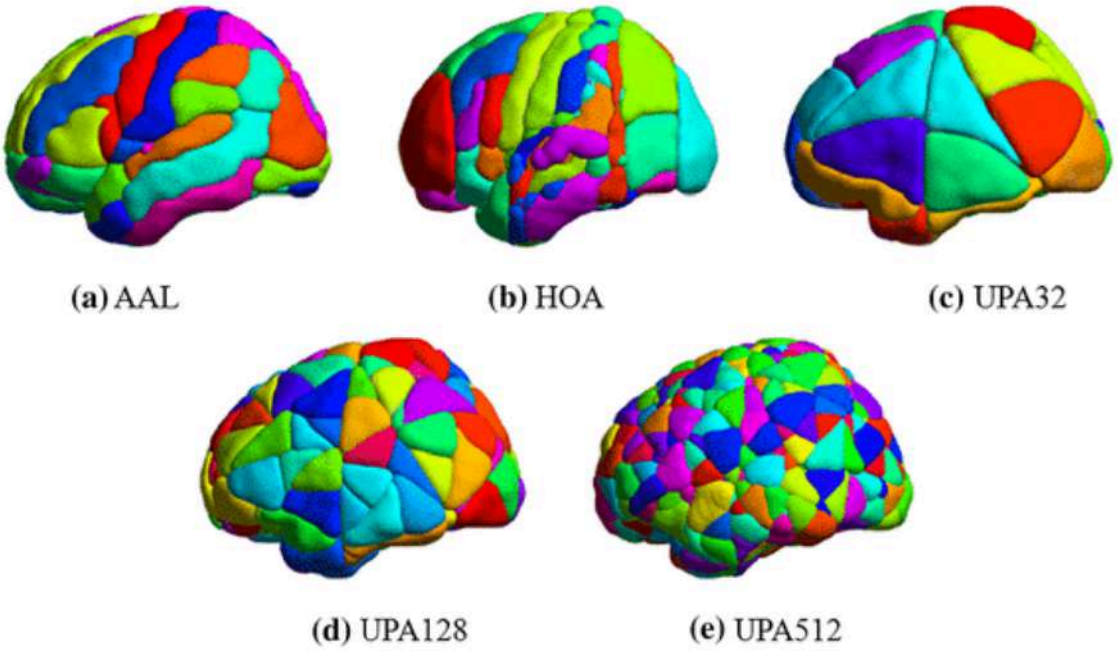

Fig 2.4.2: Parcellation atlases. Source: (Online) Experimental Brain Research [68]

2.4.3 Generation of Masks

Generating masks for fMRI data involves creating binary images that highlight regions of interest in the brain. These masks serve to focus the analysis on specific areas and exclude irrelevant or noisy data. The process typically begins with anatomical images or atlases that define brain regions. The mask can be generated manually or using automated methods based on intensity thresholds, clustering, or atlas-based segmentation. Once created, these masks are applied to the fMRI data, effectively isolating the signals from the specified brain regions. This step is crucial for enhancing the precision and interpretability of subsequent analyses, such as feature extraction and modeling, by narrowing the focus to the relevant areas of the brain.

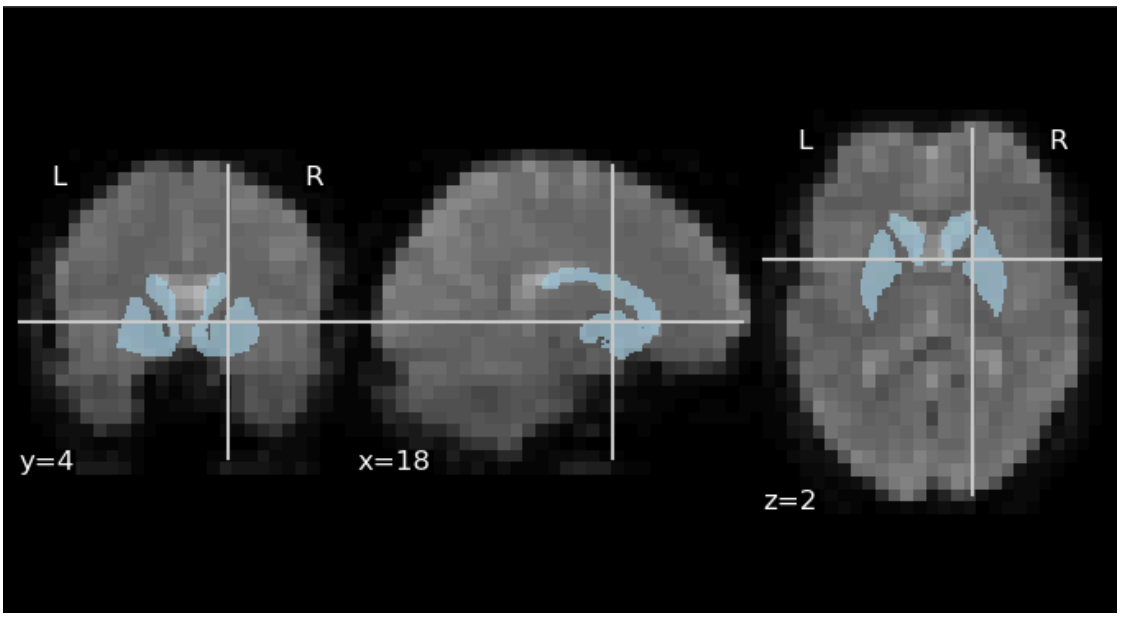

Fig 2.4.3: fMRI with mask for striatum region visualized on MRI

2.4.4 Resampling

Resampling [18] involves transforming a source image to match the dimensions and orientation of a target reference image, without altering the source image's content. This process is crucial for ensuring alignment between different imaging datasets, facilitating meaningful comparisons and analyses. The choice of interpolation method, such as 'continuous', 'linear', or 'nearest', determines how the transformation is carried out. Resampling does not modify the source image; instead, it produces a new image with the desired characteristics, including shape and affine properties, derived from the target image.

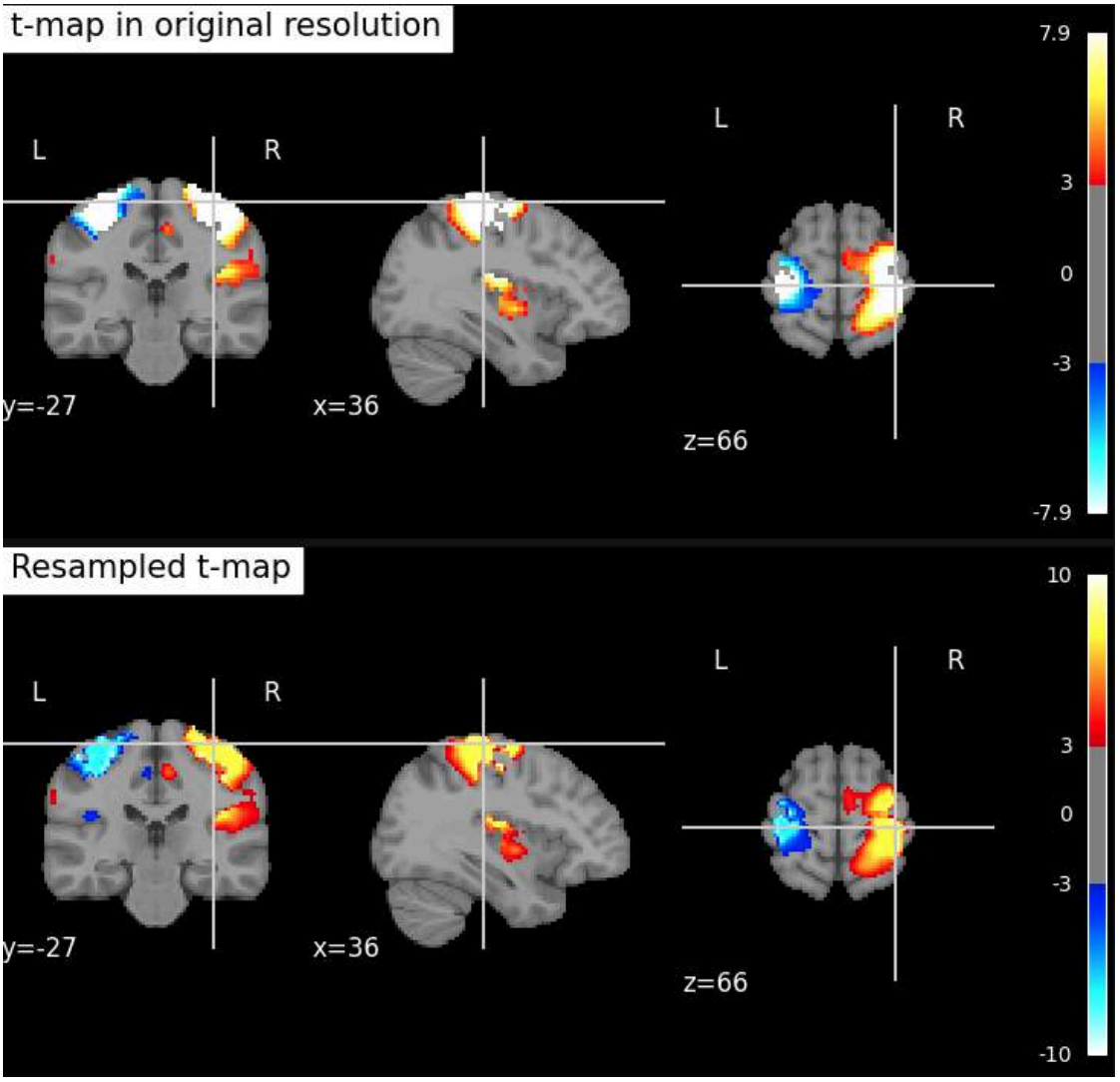

Fig 2.4.4: fMRI image and Resampled fMRI image in Nilearn. Source: (Online) Nilearn [18]

2.4.5 Smoothing

Here we smooth a mean EPI (Echo-Planar Imaging, this is the type of sequence used to acquire a functional or diffusion MRI data) image and plot the result. As we vary the smoothing [19] full width at half maximum, in a distribution, it refers to the width of a filter, expressed as the diameter of the area on which the filter value is above half its maximal value. Note how we decrease the amount of noise, but also lose spatial details. In general, the best amount of smoothing for a given analysis depends on the spatial extent of the effects that are expected.

Smoothing in fMRI preprocessing serves multiple purposes, primarily aiming to enhance data quality and facilitate robust analyses. By reducing random noise and small-scale variations, it improves the signal-to-noise ratio, aiding in the detection of genuine neural signals. Smoothing also addresses individual anatomical differences, promoting better alignment of functional data across subjects and enabling effective inter-subject comparisons.

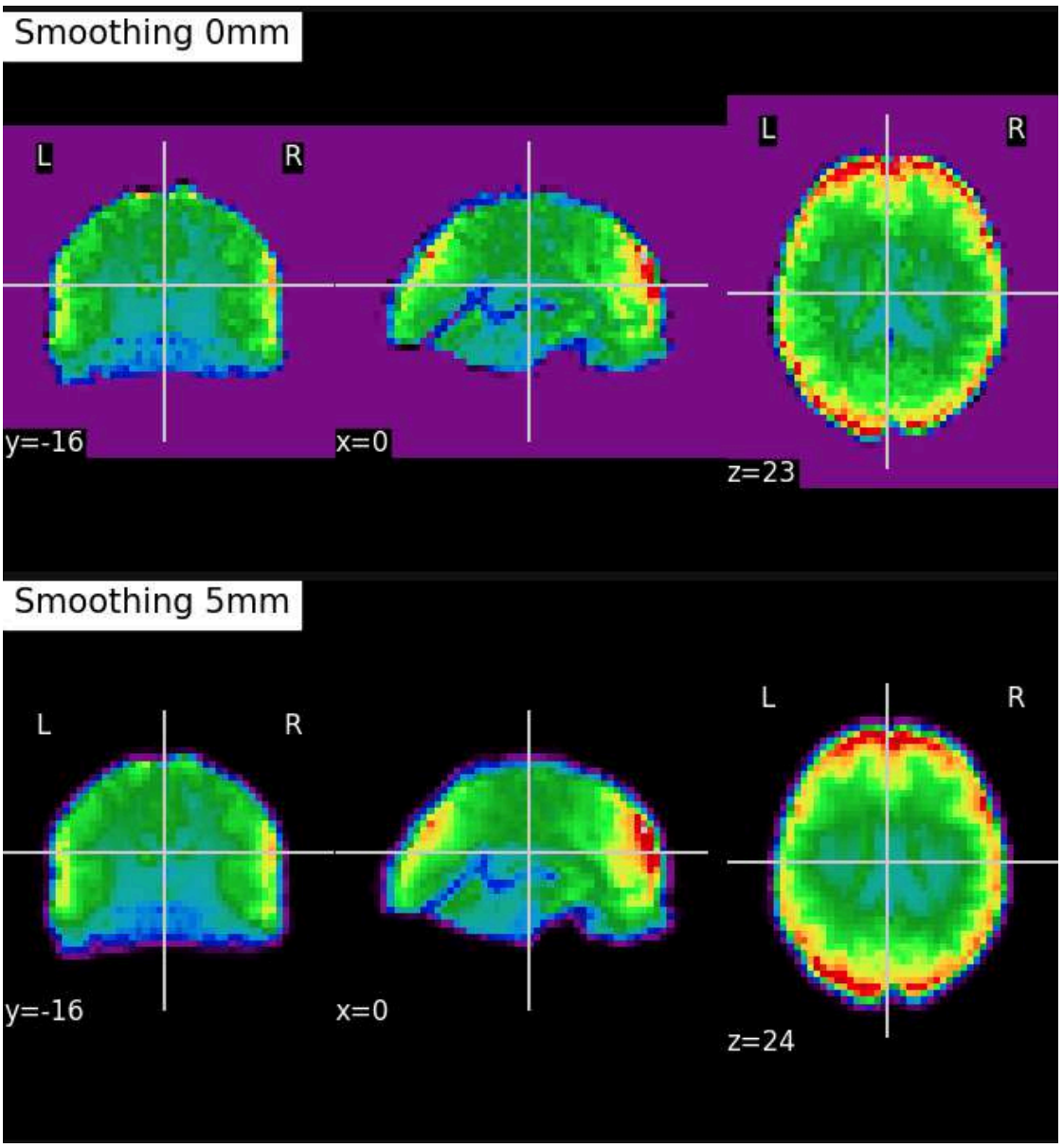

Fig 2.4.5.1: fMRI image with 0mm and 5mm smoothing. Source: (Online) Nilearn [19]

A 0mm smoothing implies no blurring, maintaining the original spatial resolution of the image. In contrast, a 20mm smoothing introduces a larger blurring effect, merging nearby voxel values and reducing fine-scale spatial details. 0mm is suitable for preserving fine anatomical structures, while 20mm may enhance signal-to-noise ratio and highlight larger-scale patterns in the data.

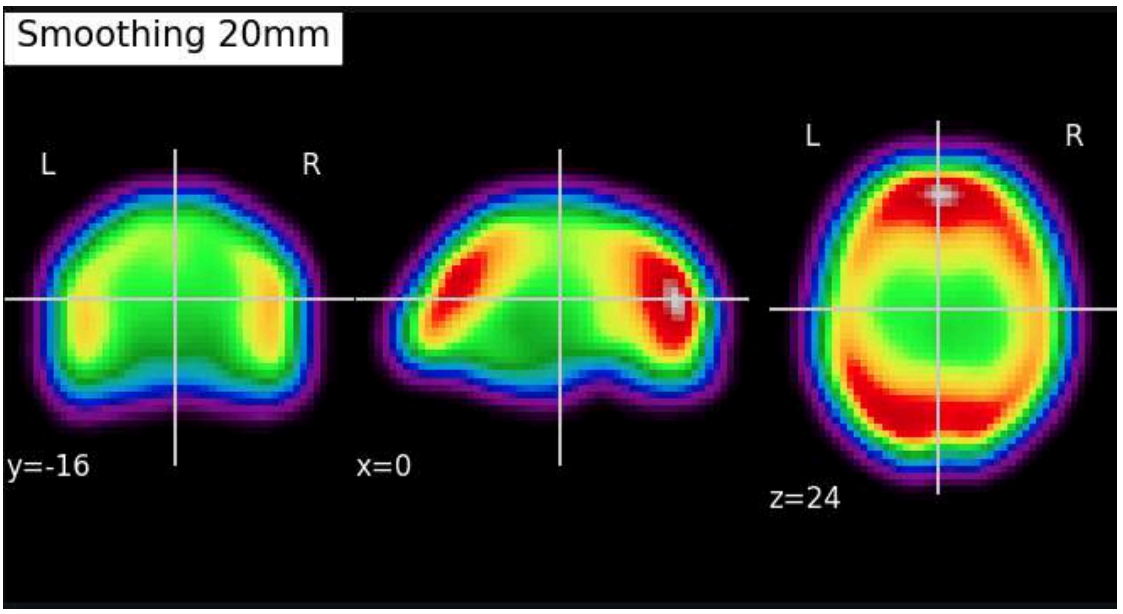

Fig 2.4.5.2 fMRI image with 20mm smoothing. Source: (Online) Nilearn [19]

2.4.6 Feature Extraction

Identifying biomarkers for schizophrenia from fMRI data, the feature extraction process [20] aims to capture neurobiological patterns associated with the disorder. The steps involved in this specific context might include:

- **Time Series Extraction:** Time series data is extracted from the masked fMRI data for specific ROIs or voxels. This involves obtaining a temporal sequence of signal intensities over the course of the imaging session.
- **Functional Connectivity:** Measures such as correlation or coherence are computed to quantify the relationship between different regions of the brain. This step reveals how activity in one region correlates with activity in another, providing insights into functional networks.
- **Frequency Analysis:** Frequency-based features such ALFF or spectral power in specific frequency bands may be calculated to capture different aspects of neural activity.

CHAPTER 3

SOFTWARE REQUIREMENT SPECIFICATIONS

3.1 Overall Description

3.1.1 Hardware Interface

The following hardware specifications were utilized in carrying out the simulation:

- Processor (CPU): A multi-core processor (e.g intel i5 or higher) is recommended to handle parallel processing efficiently.
- Ethernet connection (LAN) OR a wireless adapter (Wi-Fi)
- Hard Drive: Minimum 32 GB; Recommended 64 GB or more
- Memory (RAM): Minimum 8 GB; Recommended 16 GB or above

3.1.2 Software Interfaces

The Virtual Brain

The Virtual Brain (TVB) [33, 34] is a computational framework designed for simulating the dynamics of large-scale brain networks using biologically realistic connectivity. It utilizes tractographic data to generate connectivity matrices, defining connection strengths and time delays between network nodes. Various neural mass models are available to define the dynamics of each node. TVB simulates neural activity such as Local Field Potentials (LFP) and firing rates, as well as brain imaging data like EEG, MEG, and BOLD activations. It provides tools for connectivity and network dynamics visualization, time series analysis, and parameter exploration. TVB aims to model brain structure and function, offering insights into brain function and disorders like stroke, epilepsy, Alzheimer's, and Parkinson's. It simplifies complexity to attain macro organization, merging brain anatomy from imaging data with mathematical modeling. TVB serves as a simulation engine for clinical trials, neuroinformatics initiatives, and research facilities worldwide, supported by over 100 peer-reviewed publications.

Anaconda Navigator

Anaconda Navigator [22] is a user-friendly graphical interface bundled with the Anaconda distribution. It simplifies package and environment management for Python, crucial for data science and scientific computing. The Navigator dashboard provides quick access to tools, enabling easy package installations, updates, and environment creation. With integrated support for Jupyter Notebooks and other IDEs like Spyder, Anaconda Navigator caters to both individual developers and large-scale projects. Backed by a robust community and offering enterprise support, it streamlines the setup and maintenance of Python environments, ensuring consistency and reproducibility.

Jupyter Notebook

Jupyter Notebook [23] is an open-source, web-based environment fostering interactive and collaborative computing. Supporting various languages, it allows users to create documents with live code, visualizations, and narrative text. With its kernel system, Jupyter accommodates different programming languages within the same environment, enhancing versatility. Offering seamless integration with multimedia elements and popular data visualization libraries, Jupyter Notebooks facilitate dynamic data exploration and presentation. The ability to share notebooks in multiple formats, coupled with collaborative features, makes it a go-to tool for researchers, data scientists, and educators aiming for effective communication and reproducibility in their work.

Google Colab

Google Colab, or Colaboratory [24], is a cloud-based platform for collaborative Python coding and data analysis. Built on the Jupyter Notebook interface, it allows users to create interactive documents combining code, text, and visualizations. Colab stands out with its free access to Graphics Processing Units and Tensor Processing Units, making it particularly attractive for machine learning tasks. Operating entirely in the cloud and integrating seamlessly with Google Drive, it eliminates the need for local installations. Real-time collaboration features enable multiple users to work on the same notebook simultaneously. With support for popular Python libraries like TensorFlow, Colab is a versatile and accessible tool, facilitating collaborative projects in data science and machine learning.

3.1.3 Software Languages

Python

Python [25] is a high-level programming language renowned for its readability and simplicity. Created with a focus on code clarity, Python enables developers to express concepts in fewer lines, making it an ideal choice for both beginners and experienced programmers. Python stands as a dominant force in machine learning and data analysis due to its user-friendly syntax and a rich ecosystem of libraries. In machine learning, Scikit-Learn offers a straightforward interface for various algorithms, while TensorFlow and PyTorch excel in deep learning applications. Keras simplifies neural network development within the TensorFlow framework. For data analysis, Pandas and NumPy provide robust structures for efficient manipulation and mathematical operations, while Matplotlib and Seaborn offer versatile visualization tools. Python's readability and versatility attract both beginners and experts, fostering a thriving community.

3.1.4 Packages Used

Nilearn

Nilearn [26] is a Python library tailored for processing and analyzing fMRI data. It simplifies the complexities of neuroimaging tasks with features like preprocessing,

connectivity analysis, statistical tools, and machine learning integration. Nilearn facilitates efficient data handling, enabling users to explore FC patterns, conduct statistical analyses, and build predictive models. With seamless integration into popular neuroimaging libraries, Nilearn is a valuable resource for researchers seeking insights into brain activation, connectivity, and cognitive states. Its user-friendly interface and visualization tools make it accessible to both beginners and seasoned neuroscientists, contributing to advancements in fMRI research and our understanding of the human brain.

Scikit-Learn

Scikit-Learn, or sklearn [27], is a widely-used machine learning library for Python known for its simplicity and efficiency. It provides a diverse set of tools for tasks like classification, regression, and clustering, featuring popular algorithms such as SVM and Random Forests. With a consistent API, it's easy to experiment with different models. Scikit-Learn offers functions for data preprocessing, model evaluation, and seamless integration with NumPy and SciPy. Its active community and extensive documentation make it a reliable choice for both beginners and experienced data scientists, facilitating predictive modeling and analysis in various fields.

TVB-Python

The console version of TVB [36] provides a powerful programmatic interface for interacting with TVB. Unlike the graphical user interface (GUI), it's not designed for remote use but is ideal for building reproducible workflows and detailed scripting. It records precise actions and provides full access to TVB's APIs, allowing researchers and developers fine-grained control over simulations and analyses. TVB offers several flavors of scripting interfaces, differing in the shell used and the number of TVB services utilized. The console interface is a valuable tool for those who require more control and automation in their TVB workflows.

Matplotlib

Matplotlib [61] is a Python library for creating static, interactive, and animated visualizations. With a MATLAB-like interface, it offers a wide array of plot types including line plots, scatter plots, bar charts, histograms, and more. Its extensive customization options enable users to fine-tune every aspect of their plots, from colors and line styles to annotations and axes. Interactive features like zooming and panning aid in data exploration. Its object-oriented API fosters extensibility, allowing users to develop custom plot types and functionalities. Extensively documented with tutorials and examples, it ensures easy adoption and learning.

CHAPTER 4:

IMPLEMENTATION

4.1 Validation of Biomarkers

To assess the efficacy of the biomarker proposed in [1], we looked to replicate their results. While the code was freely available on GitHub, there was a need to obtain an independent dataset to perform the analysis. The COBRE dataset sample [31] available in the International Neuroimaging Data-sharing Initiative was of interest as it provided pre-processed fMRI data of patients diagnosed with schizophrenia and healthy controls. The original dataset was released under the Creative Commons Attribution Non-Commercial license making it available for use in our study.

4.1.1 Description of dataset

The dataset comprises pre-processed resting-state fMRI obtained from 72 patients diagnosed with schizophrenia (58 males, age range = 18-65 years) and 74 healthy controls (51 males, age range = 18-65 years). Each subject's fMRI dataset is provided as a single nifti file (.nii.gz), consisting of 150 EPI blood-oxygenation level dependent (BOLD) volumes acquired over 5 minutes (TR = 2 s, TE = 29 ms, FA = 75°, 32 slices, voxel size = 3x3x4 mm^3, matrix size = 64x64, FOV = mm^2). Pre-processing was done using the NeuroImaging Analysis Kit (NIAK) version 0.12.14, executed on CentOS version 6.3 with Octave version 3.8.1 and the Minc toolkit version 0.3.18. This data was sourced from [31].

For each patient the following data was included:

1. Resting fMRI
2. Anatomical MRI
3. Phenotypic data in the form of TSV (Tab Separated Value file) for every participant including: gender, age, handedness, diagnostic information, subject type (i.e, patient or control).

4.1.2 Replicating FSA score

For computing the Functional Striatal Abnormalities (FSA) score [1], the following three features of the striatum required to be computed:

1. Intra-striatal FC
2. Extra-striatal FC
3. Striatal fALFF

fALFF provides insights into the magnitude of spontaneous neural activity at rest, with higher fALFF values indicating greater low-frequency fluctuations and potentially more pronounced neural activity.

Initially we were required to resample the striatum mask provided by the researchers [58]. Resampling involves adjusting the spatial attributes, such as voxel size, orientation, and field of view, of the mask to align with those of the fMRI images in our dataset. We then proceeded to feature extraction. While the code provided included the computation of Intra-striatal FC and Extra-striatal FC, we were required to compute striatal fALFF. Towards this we referenced from [59] which provided a definition of fALFF from which striatal fALFF for each subject based on this definition was calculated.

Following feature extraction, a SVM classifier is applied for classification. The dataset undergoes an 80-20 train-test split using the 'train_test_split' function from Scikit Learn, ensuring 80% for training and 20% for testing, with a fixed random seed for reproducibility. Feature scaling using 'StandardScaler' is applied to normalize feature values, ensuring consistent input for the SVM classifier. To address potential variability due to the train-test split, the process is repeated 10 times without a fixed seed, resulting in a mean accuracy of 64.13%.

Following initial model training, a thorough hyperparameter tuning process is executed using GridSearchCV to optimize the SVM classifier's performance. The parameter grid encompasses various SVM kernel types ('sigmoid', 'linear', 'rbf'), gamma values, and the regularization parameter (C), with logarithmic scales applied to gamma and C for comprehensive exploration. GridSearchCV is initialized with the SVM classifier, the defined parameter grid, 13-fold cross-validation, and parallel processing for efficiency.

Subsequently, the optimized model is used to predict labels for the test set, resulting in an accuracy of 72.4%. Thus validating the FSA score with a suitable efficacy in classification of schizophrenia and healthy subjects.

4.1.3 Further analysis of striatal fMRI

As elucidated in [1], [3], [16], the striatal region of the brain was found to be of much significance in differentiating schizophrenic patients from healthy controls. To this end, we aimed to use Nilearn’s built in Support Vector Classifier (SVC), to classify schizophrenic patients and healthy controls in the COBRE dataset by focusing on the striatum. The difference between a conventional SVM and Nilearn’s SVC lies in the unique ability of Nilearn’s decoder to take 3-dimensional fMRI images directly as input. This is in contrast with [1], where the researchers quantified specific striatal features numerically and then fed it into Sklearn’s SVM.

The initial steps of the procedure followed is similar to the procedure provided by [1] of defining the striatal mask, resampling the mask to a sample fMRI image and visualizing the same. Since the fMRI file is in 4-dimensional (Fig 4.1.3.1), the ‘mean img’ function is used to compute the mean of images of a given subject over time which is the 4th dimension, thus converting it to 3 dimensions.

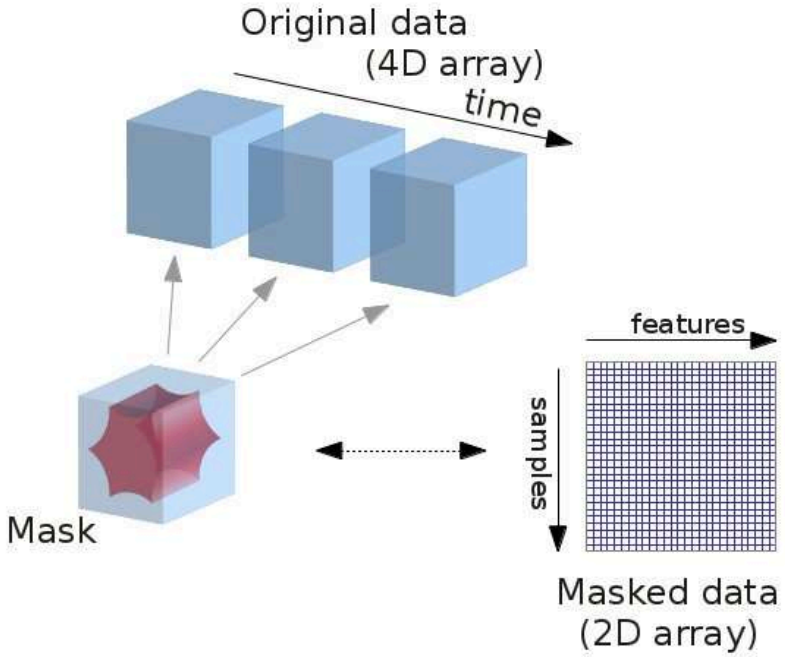

Fig 4.1.3.1: Masking data: from 4D Nifti images to 2D data arrays. Source: (Online) Nilearn [57]

The next step is training a SVM model which is done by using nilearn decoder which is a predefined SVM model. The parameters for the model include the estimator and mask. The model is fit using decoder.fit() which was predefined to instantiate the Decoder. It takes the mean-fMRI images as input learning data and Subject Type as the class label. To find the best accuracy, a loop was initiated to loop over different slices; the first n participants were taken for training and the remaining to test the decoder model as demonstrated in Fig 4.1.3.2 .

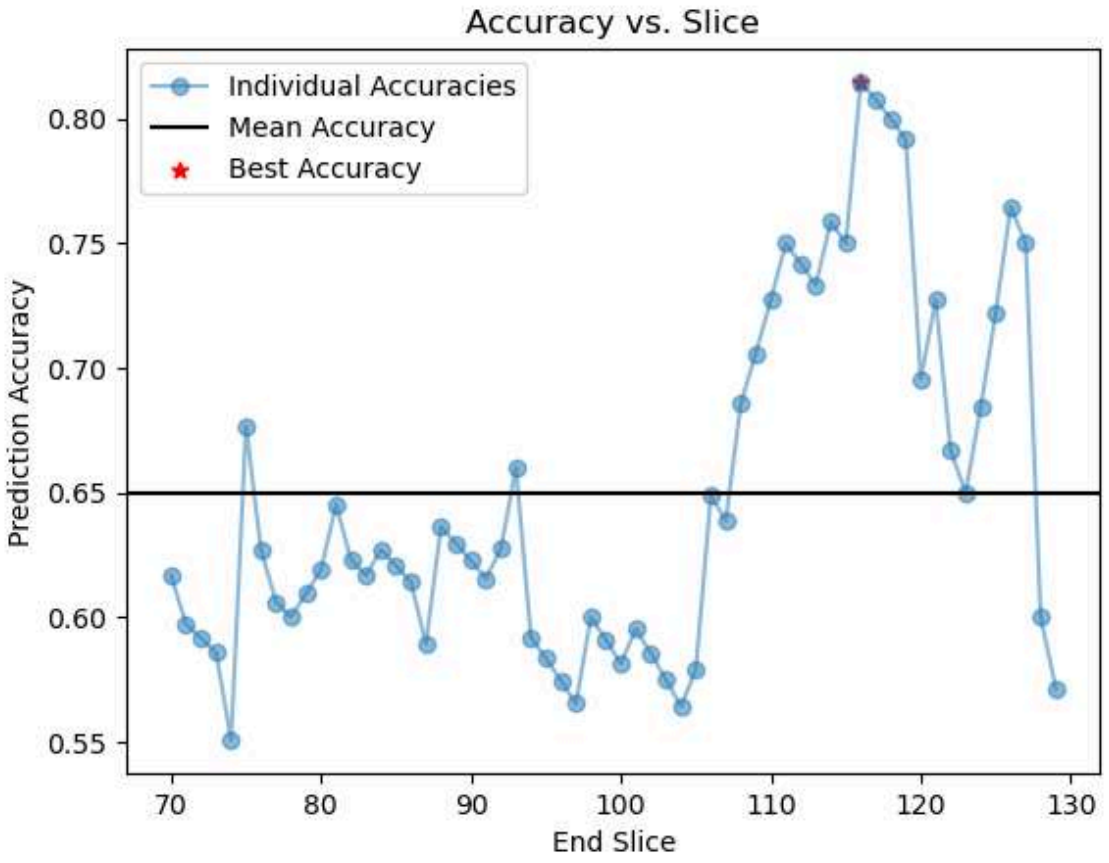

Fig 4.1.3.2: Accuracy v/s train-test slice

The best prediction accuracy was found to be 81.5% over slice 116. Furthermore, K-fold Cross Validation was used to evaluate the model performance on different subsets of the data resulting in a global maxima accuracy of 75% with an average accuracy of 65.2%. The SVM weights used to train the model are plotted on a sample fMRI using the 'plot_stat_map' function as illustrated in Fig 4.1.3.3 . The correlation between SVM weights is a measure of the similarity or linear relationship between the weights associated with different features (voxels in the case of fMRI data) in the model. A high positive correlation indicates that the weights move in the same direction (both increase or decrease together), while a high negative correlation indicates that the weights move in opposite directions.

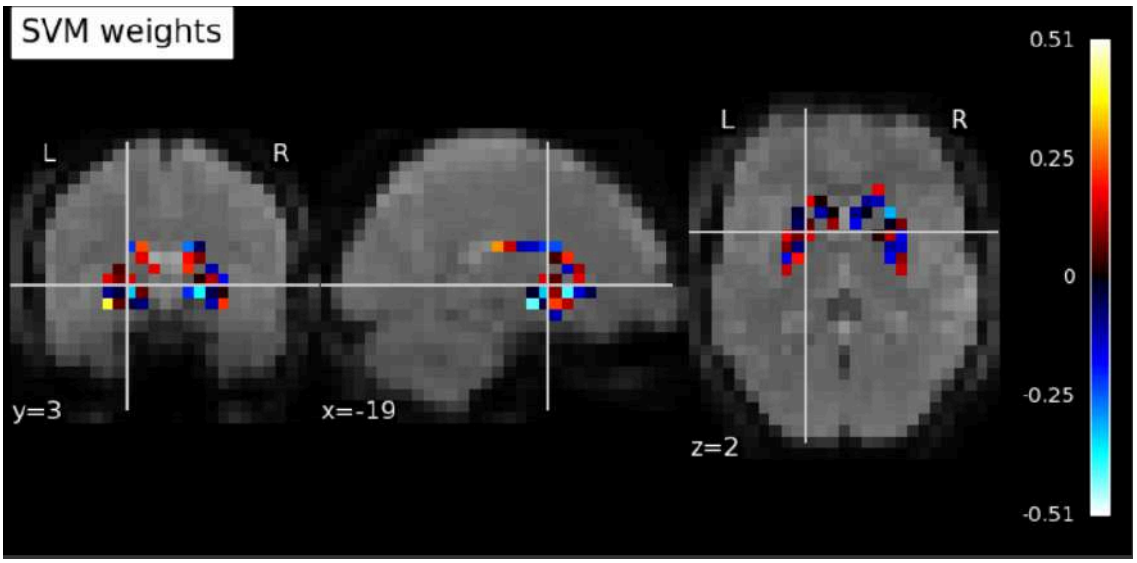

Fig 4.1.3.3: SVM weights plotted on fMRI with mask of striatum

Preserving the time dimension

Here, we looked to preserve the temporal aspect of our fMRI which we were previously collapsing by taking the mean over time. To facilitate further analysis, the Nilearn's apply mask() function is employed, allowing the conversion of the 4D NiFtI image into a structured 2D array, organized as (time series, voxels) as illustrated in Fig 4.1.3.1. After acquiring the 2D array, the subsequent step involves feeding it into the SVM to obtain accuracy. Here, a challenge emerged: the SVM necessitates a 1D array, whereas our data assumed a 2D structure. To bridge this gap, we used the flatten() function. Flattening an array refers to the process of transforming a multi-dimensional array into a one-dimensional array by collapsing all of its dimensions. This transformation appends subsequent rows to the end of the initial row seamlessly converting the 2D array into the requisite 1D format, thereby facilitating the input compatibility demanded by the SVM. Despite the loss of temporal structure, SVMs can effectively learn decision boundaries from flattened fMRI data, especially when the relevant spatial patterns are captured in the intensity values. Upon transforming the 2D array into a requisite 1D format, the subsequent step involved training a SVM model, employing a train-test split ratio of 0.2. The initial model training yielded an accuracy of 72.4%. Next the average accuracy across 10 independent runs was computed, yielding an average accuracy of 68.9%. Furthermore, to optimize the SVM model parameters, we employed Grid Search, an advanced hyperparameter tuning technique. The optimal parameters, as determined by GridSearchCV, were found to be 'C': 166.81, 'gamma': 1.75e-06, 'kernel': 'sigmoid', resulting in an accuracy of 79.3%.

Application of Convolution Neural Networks

As opposed to flattening or averaging the temporal dimension of the fMRI, we looked at classification models that were able to retain dimensionality. fMRI data is inherently multidimensional, comprising spatial and temporal dimensions that collectively encode complex neural activity patterns. CNNs excel in processing multidimensional data [32], making them well-suited for analyzing fMRI datasets.

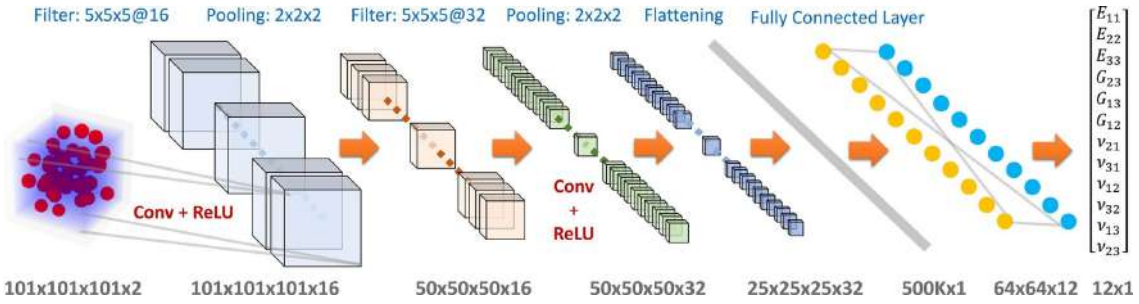

.**Fig 4.1.3.4:** CNN Architecture. Source: Rao, C. et al. 2020 [60]

A CNN was designed consisting of a series of layers designed to extract and process features from the input fMRI data (Fig 4.1.3.4). It begins with a 3D convolutional layer (Conv3D) employing 32 filters, each with a kernel size of (3, 3, 3), and ReLU activation function. This is followed by a 3D max-pooling layer (MaxPooling3D) with a pool size of (2, 2, 2) to reduce spatial dimensions and capture essential features. Another convolutional layer with 32 filters and a kernel size of (3, 3, 3) is added, followed by another max-pooling layer with the same specifications. The output is then flattened into a one-dimensional array and fed into a fully connected dense layer (Dense) with 64 neurons and ReLU activation. Finally, an output layer with a single neuron and sigmoid activation function is employed for binary classification. This architecture is tailored to classify subjects into Healthy Control or Patient categories based on fMRI data. The model underwent training across various test sizes to identify the optimal accuracy split. A maximum accuracy of 72.4% was achieved with a 60-40 train-test split. Following this, a confusion matrix was plotted, revealing 23 patients correctly classified as Healthy and 19 classified as schizophrenic.

4.2 Towards simulation

We chose to use TVB as our simulation tool owing to its extensive capabilities aligned with our goal of simulating whole-brain dynamics through large-scale brain network models. TVB provides both a Graphical User Interface (GUI) which provides a plethora of intuitive visualization as well as a Python library allowing for robust analysis and computation.

4.2.1 Input to TVB

TVB takes as input a 'Connectivity' file which contains a detailed description of the structural connectivity of the brain that aims to quantify the strength of signal transmission between regions. One can provide their own connectivity by processing multimodal MRI through a dedicated pipeline designed for TVB [12]. Additionally, TVB also provides a series of connectivity datasets which are readily usable, each mapping a different number of regions. These connectivities are primarily derived from the CoCoMac database and are processed to generate a series of text files which TVB uses to inform the structural aspect of large-scale brain simulation.

We chose to use the Connectivity-96 dataset [45] available in TVB, that provided a suitable level of resolution in region mapping that enabled us to show region-level aberrations. This dataset contains 82 cortical and 14 subcortical regions of interest.

A description of the components of Connectivity-96 dataset

- **weights.txt**: A 96x96 matrix representing connectivity weights between brain regions. It represents structural connectivity constructed using diffusion weighted MRI (dwMRI) tractography.
- **tract_lengths.txt**: A 96x96 matrix providing the average length of fiber tracts in millimeters between each pair of brain regions. It is used to compute the transmission delay in signal transmission.
- **info.txt**: Contains units for quantities, particularly the area, expressed in square millimeters (mm^2).
- **cortical.txt**: A vector of 96 integer values. Each value indicates whether the corresponding brain region is cortical (1) or subcortical (0).
- **centres.txt**: Consists of 96 rows and 4 columns.
    - Column 1: Unique ID for each brain region.
    - Columns 2, 3, 4: x, y, z cartesian coordinates of the center point of each region. If white matter fiber lengths are unavailable, TVB computes a tract lengths matrix based on the Euclidean distance between region pairs using this information.
- **average_orientation.txt**: Contains 96 rows and 3 columns. Each row represents the coordinates for the orientation of the center point of a brain region.
- **areas.txt:**Provides the surface area in square millimeters of each brain region.

4.2.2 Simulation parameters in TVB

TVB requires configuring the following parameters in order to execute a simulation:

1. **Long-range connectivity**: Long-range connectivity is the pre-processed structural connectivity data. ex. Connectivity-96
2. **Conduction Speed**: Specifies the speed at which the signals can travel from one region to another.
3. **Coupling**: Allows the user to specify the global coupling scheme (linear, sigmoidal, etc) between nodes in the network.
4. **Cortical Surface**: If a surface-based simulation is required, it is necessary to load a cortical surface dataset. If one is performing a region-based simulation, leave this unchecked.

5. **Spatiotemporal stimulus**: This allows us to specify some stimulus that varies with time for the model that can be configured in the 'Stimulus Tab'.

6. **Local Dynamic Model**: This allows us to choose one of the several neural mass models available in TVB. Additionally, we also set the values for the various parameters used in the neural mass model.

7. **Integration scheme**: This allows us to choose the integration scheme that will produce a numerical solution to the set of differential equations of the neural mass model.

8. **Integration step-size**: This defines how frequently a solution to the differential equations of the neural mass model is to be produced. A smaller step size will result in better accuracy but an increased compute time.

9. **Monitors**: Monitors allow us to specify what output we want the simulation to provide. TVB can output Raw Recording, Temporal Sub-Sample, EEG, MEG, Intracerebral / Stereo EEG BOLD, etc.

10. **Simulation length**: This defines how long the brain activity would be simulated for.

11. **PSE (Parameter Space Exploration)**: Optionally TVB provides a feature to produce multiple simulations by specifying the range of values of particular parameters.

4.2.3 Jansen-Rit Neural Mass Model

Neural mass models describe the activity produced within a single node (which can be a region in the case of the region-based simulations or a vertex of the surface triangles as in surface-based simulations in TVB). Our goal is to simulate large-scale brain activity i.e, whole-brain activity, therefore, it is not computationally feasible to simulate the activity of each individual neuron as there are roughly 86 billion of them in the brain. We instead group multiple neurons in what is called a neural mass or neural population. Within this grouping, we may look to differentiate neurons based on their type for example Excitatory and Inhibitory. Therefore the activity of the neural mass can be expressed using a simplified model that describes the average/mean behavior of each of these groups. Mathematically, the activity of these individual neural masses is quantified by expressing the model as a set of differential equations that describes the change of some biophysical quantity such as membrane potential, firing rate, etc. with respect to time. These are thus called neural mass models. TVB provides several such neural mass models.

We chose to use the Jansen-Rit Neural Mass Model [40] for our study, owing to the fact that it is well-established in the field of simulation and has been deeply studied. This model is particularly focused on capturing the dynamics of excitatory and inhibitory interactions within neuronal populations. The model consists of a set of differential

equations that describe how the membrane potentials of excitatory and inhibitory neurons evolve over time in response to inputs and feedback from other neurons.

A)

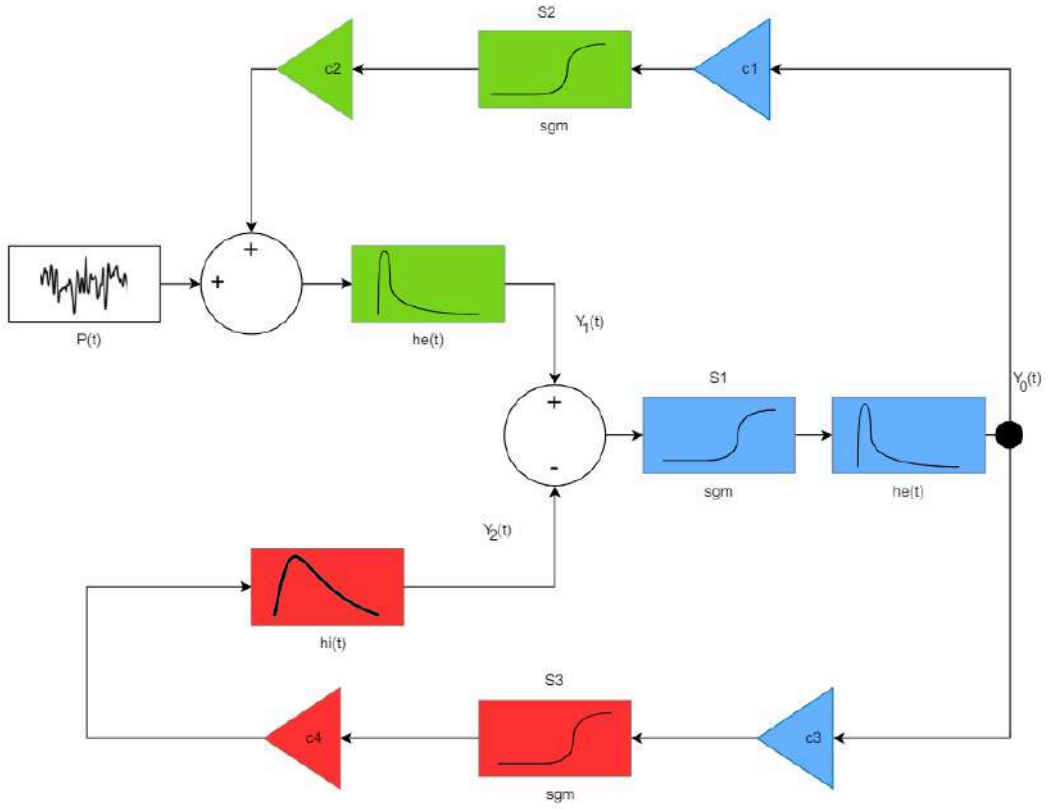

B)

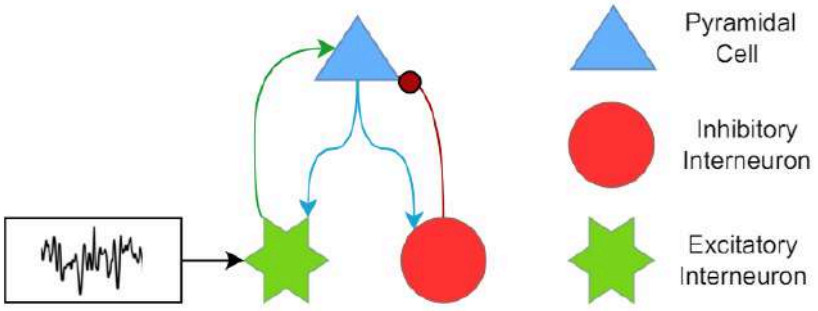

Fig 4.2.3.1: (A) Jansen Rit Model. (B) Diagram of Jansen and Rit model for a cortical column, each color and shape represent one type of column population: pyramidal (blue), excitatory interneuron (green) and inhibitory interneuron (red). Inspired by Roser Sanchez-Todo et al 2018 [69]

The Jansen-Rit model describes the dynamics of a small cortical region by considering three interconnected neural populations: excitatory interneurons , pyramidal cells, and inhibitory interneurons. The model aims to replicate the spontaneous EEG alpha oscillations and the responses observed in evoked potentials following pulsatile input.

The model receives external input (p) representing excitatory and inhibitory inputs, respectively, from outside the local cortical region. The inputs are then processed by linear filter boxes (he(t) and hi(t)) representing the mean response of excitatory and inhibitory synapse populations, respectively. These filters describe the time course of the population mean of postsynaptic potentials, considering synaptic and dendritic dynamics. The filtered inputs contribute to the mean membrane potentials of the excitatory, pyramidal, and inhibitory interneuron populations. The inhibitory input negatively affects the membrane potential of the pyramidal population. The mean membrane potentials are then passed through a sigmoid function (Sgm(v)) to determine the mean output firing rate of each neural population. This sigmoid function incorporates the dispersion of responses due to variability in parameters and neuronal states. The model contains a number of useful relationships between the connectivity constants c1 to c4. These constants that act as amplifiers of sorts, are proportional to the average number of synapses between the pyramidal cells and the excitatory and inhibitory feedback elements. The primary output of the model is taken as the difference between the mean potentials of the pyramidal population and the inhibitory input. This represents the net activity of the pyramidal cells and serves as the output signal of the model.

Jansen-Rit Model equations

The following equations were referenced from the Jansen Rit 1995 model [55].

$$\dot{y}_0(t) = y_3(t)$$

$$\dot{y}_3(t) = Aa\, Sigm\left[y_1(t) - y_2(t)\right] - 2ay_3(t) - a^2 y_0(t)$$

$$\dot{y}_1(t) = y_4(t)$$

$$\dot{y}_4(t) = Aa\left\{p(t) + C_2 Sigm\left[C_1 y_0(t)\right]\right\} - 2ay_4(t) - a^2 y_1(t)$$

$$\dot{y}_2(t) = y_5(t)$$

$$\dot{y}_5(t) = Bb\left\{C_4 Sigm\left[C_3 y_0(t)\right]\right\} - 2by_5(t) - b^2 y_2(t)$$

where,

$$Sigm(\nu) = \frac{2e_0}{\left[1+e^{r(\nu_0-\nu)}\right]}$$

In the above equations, each state variable (y_n) provides an output measuring the following:

y0- pyramidal cell postsynaptic membrane potential.

y1- excitatory interneuron post-synaptic membrane potential.

y2- inhibitory interneuron post-synaptic membrane potential.

y3- pyramidal cell population firing rate.

y4- excitatory interneuron firing rate.

y5- inhibitory interneuron firing rate.

Sigma**[*v*]**- sigmoidal activation function.

Configurable parameters

The following are the parameters of the Jansen Rit model that can be configured in TVB [72].

A: Maximum amplitude of Excitatory Postsynaptic Potentials (EPSP) in millivolts (mV). Also known as the average synaptic gain.

B: Maximum amplitude of Inhibitory Postsynaptic Potentials (IPSP) in mV. Also known as the average synaptic gain.

a: Reciprocal of the time constant of passive membrane and all other spatially distributed delays in the dendritic network, in $milliseconds^{-1}$. Also known as the average synaptic time constant.

b: Reciprocal of the time constant of passive membrane and all other spatially distributed delays in the dendritic network, in $milliseconds^{-1}$. Also known as the average synaptic time constant.

v_0: Firing threshold (PSP) for which a 50% firing rate is achieved. It represents the value of the average membrane potential corresponding to the inflection point of the sigmoid, in mV.

μ_{max}: Determines the maximum firing rate of the neural population, in $seconds^{-1}$.

r: Steepness of the sigmoidal transformation, measured in mV^{-1}.

J: Average number of synapses between populations.

p_min: Minimum input firing rate.

p_max: Maximum input firing rate.

μ: Mean input firing rate.

4.2.4 Simulating region-level dysfunction

TVB provides the unique ability to define different configurations of the same neural mass model and apply these configurations to different regions. This approach would thus be useful to simulate region-level dysfunction. We looked to identify regions in the Connectivity-96 that were analogous to the dysfunctioning regions identified in the literature survey in Section 2.2.

Towards this end, we defined 3 different configurations of the Jansen Rit Model.

1. Default Configuration- This configuration is representative of normal resting state brain activity as specified in [40].
2. Increased activity- This configuration is created by increasing the excitatory parameters ‘c1’ and ‘c2’ of the Jansen Rit Model leading to increased activity
3. Decreased activity- This configuration is created by increasing inhibition parameters ‘c3’ and ‘c4’ of the Jansen Rit Model leading to decreased activity.

Table 4.2.4.1 lists the regions that were altered with the increased and decreased activity configurations. It is to be noted that in TVB, the nomenclature has been marginally altered in that ‘c1’, ‘c2’,’c3’,’c4’ is represented as ‘α1’, ’α2’, ‘α3’, ‘α4’. Each of these terms by default are represented using a single value that is applied to all the nodes i.e, regions of the model. However, in order to show varied values across regions, TVB requires an array of 96 values to be provided, allowing one to set a unique value for each of the 96 regions.

Parameter	**Value**	
A	3.25	
B	22.0	
a	0.1	
b	0.05	
v_0	5.52	
v_{max}	0.0025	
r	0.56	
J	135.0	
C_1	1.0	1.25
C_2	0.8	1.0
C_3	0.25	0.31
C_4	0.25	0.31
p_{min}	0.12	
p_{max}	0.32	
μ_{max}	0.22	

Table 4.2.4.1: Configuration of parameters for the initial execution of the Jansen-Rit Model simulation

Increased activity regions	**Reduced activity regions**
Orbital Inferior prefrontal cortex	Posterior cingulate cortex
Orbitomedial prefrontal cortex	Medial prefrontal cortex
Orbital Lateral prefrontal cortex	Parahippocampal cortex
Anterior visual area, ventral part	Medial premotor cortex
Visual area 2 (secondary visual cortex)	Anterior cingulate cortex
Anterior visual area, dorsal part	Inferior parietal cortex
Visual area 1 (primary visual cortex)	Medial parietal cortex
Secondary somatosensory cortex	Intraparietal cortex
Primary somatosensory cortex	Superior parietal cortex
Ventrolateral premotor cortex	Superior temporal cortex
Primary motor cortex	Anterior insula
Dorsolateral premotor cortex	Posterior insula
Frontal eye field	Dorsomedial prefrontal cortex
	Ventrolateral prefrontal cortex
	Dorsolateral prefrontal cortex

Table 4.2.4.2: Regions tweaked to show increased or reduced activity based on prior studies reviewed in Section 2.2

4.2.5 Coupling and Integration scheme

In order to define the nature of synchrony between two regions in the brain network model, a coupling scheme is defined. TVB supports several coupling schemes like Linear, Sigmoidal, etc. However a special **sigmoidal coupling scheme** exists built to be used specifically with the Jansen-Rit model. The equation for the coupling is defined as follows:

$c(x) = cmin + (cmax - cmin)/1.0 + exp(-r(x - midpoint)/\sigma)$
Source: Jansen-Rit Sigmoidal Coupling Scheme TVB [73]

This equation describes how neuronal populations interact within the cortical network, with the coupling strength modulated sigmoidally by the input variable x. The parameters of the functions are:

$cmin$: Represents the minimum coupling strength, defining the baseline level of interaction between neuronal populations.

$cmax$: Denotes the maximum coupling strength, indicating the upper limit of connectivity within the neural network.

$midpoint$: Specifies the midpoint of the sigmoidal curve, delineating the transition point where the coupling strength begins to rise significantly.

r: Represents the steepness of the sigmoidal transformation, influencing the rate at which the coupling strength changes in response to variations in the input.

a: Represents the scaling factor applied to the coupling term, adjusting the overall magnitude of the coupling effect.

Stochastic Integration
Since the Jansen Rit model is represented as coupled second-order nonlinear ordinary differential equations, an integration scheme is required to solve and produce solutions to the differential equations. TVB provides several deterministic and stochastic integration schemes. Stochastic integration is a computational technique employed to simulate systems influenced by random fluctuations or noise. In the context of neural modeling, stochastic integration accounts for the inherent variability observed in neural activity due to factors such as synaptic noise and spontaneous neuronal firing. Unlike deterministic integration methods, which yield fixed trajectories, stochastic integration introduces randomness into the system, enabling the simulation of probabilistic behaviors inherent in the brain. Given the nature of our study in simulating a diseased brain we chose to use the **Heun-Stochastic integration scheme** [51].

4.2.6 Generating BOLD and Functional Connectivity

The BOLD signal is a measure commonly used in fMRI to infer neural activity in the brain. It relies on the principle that changes in neural activity lead to changes in local blood flow and oxygenation levels, which can be detected by fMRI. The BOLD signal is based on the differential magnetic properties of oxygenated and deoxygenated hemoglobin. Oxygenated hemoglobin is diamagnetic and leads to a slight decrease in the local magnetic field, while deoxygenated hemoglobin is paramagnetic and leads to a slight increase in the local magnetic field. These changes in magnetic properties alter the MR signal detected by the scanner. By monitoring these changes in MR signal, fMRI can indirectly measure neural activity in different brain regions. Increases in the BOLD signal are interpreted as increases in neural activity, while decreases may indicate decreases in activity or changes in neuronal processing. We thus looked to generate a simulated BOLD signal for our brain network model which incorporated the region-level dysfunction.

While the Jansen-Rit model simulates neural activity which is represented as firing rates or membrane potentials, there is a need to map this neural activity to a simulated BOLD signal. The Balloon-Windkessel [48] model is widely used for this purpose, taking as input neural activity and mapping it to a BOLD signal. However due to the computational cost associated with the Balloon-Windkessel model, TVB offers a simplified computational approach for generating simulated BOLD time series, which is particularly useful for comparing with empirical data. Instead of directly implementing the complex differential equations of the Balloon-Windkessel, TVB employs a Volterra Kernel approximation [49]. Conceptually, it describes a damped oscillatory wave, characterized by parameters such as the exponential decay rate and oscillatory frequency, which govern the temporal dynamics of the hemodynamic response that is calculated periodically [50]. The period is typically a multiple of 500 ms; most studies used a period of 2000 ms.

TVB encompasses outputs within ‘monitors’ which can be specified prior to executing a simulation. We utilized two monitors:

- BOLD Monitor: This monitor captures BOLD signals estimated by the Volterra Kernel.
- Temporal Average Monitor: By computing temporal averages of neural activity, this monitor offers a broader perspective on the overall dynamics of the simulated brain activity.

The output of the BOLD monitor is structured as a four-dimensional array i.e, (time, state variable, region, mode). Here ‘time’ represents the number of BOLD signal calculations is determined by the simulation length divided by the BOLD period. There are 4 state variables for the Jansen-Rit Model ('y0', 'y1', 'y2', and 'y3') and 96 region outputs in total. Notably, for the Jansen-Rit Model, the mode remains constant at 1 since it is not multi-modal.

In order to compute the resultant BOLD signal, we consider the net excitatory population's output. This is the difference between 'y1' and 'y2' [43]. By calculating the difference between these two variables, we isolate the excitatory component of neural activity, which is essential for accurately characterizing FC patterns. Subsequently, we looked to obtain a steady signal by discarding the initial fluctuations in the signal inspired by similar studies [47]. To remove transient time from our simulation data, we apply a slicing operation to the arrays containing the BOLD signals and the BOLD time series. Specifically, we discard the initial portion of the data, which corresponds to the transient period at the beginning of the simulation. By removing these transient fluctuations, we ensure that our analysis focuses on the steady-state behavior of the neural network, providing a more accurate representation. Once the transient fluctuations are removed, we utilize TVB's TimeSeries Region method to generate a resultant time series sampled at 1ms, providing a smooth signal as opposed to the discretized signal caused by the periodic nature of the BOLD signal calculation.

Functional Connectivity Matrix Computation:
Since we now have a resultant BOLD time-series we can now compute a FC matrix. In practical terms, FC is often represented as a matrix, where each cell represents the strength of the statistical correlation between two brain regions. There are several methods for computing this statistical similarity including Pearson's Correlation, Cross correlation, Partial Correlation, etc [52]. We chose to use Pearson's Correlation Coefficient provided in Numpy [53]. The resulting FC matrix, structured as a 96x96 array, represents the statistical similarity of the BOLD signal between all pairs of brain regions. We then use Nilearn's 'Plot Matrix' function to plot the resultant FC matrix along with the region labels.

4.2.7 Outputs of the simulation

The outputs of the simulation have been illustrated in Fig 4.2.7.1 and Fig 4.2.7.2. shows the BOLD signal that has been simulated for the 96 regions for the simulation length specified i.e 20 seconds with the removal of the initial fluctuations. Fig 4.2.7.1 is the FC matrix generated by computing the Pearson correlation coefficient between every region's BOLD time series to the rest.

The simulated FC was compared to empirical FC using the Mean Squared Error (MSE) metric, which was found to be 0.18.

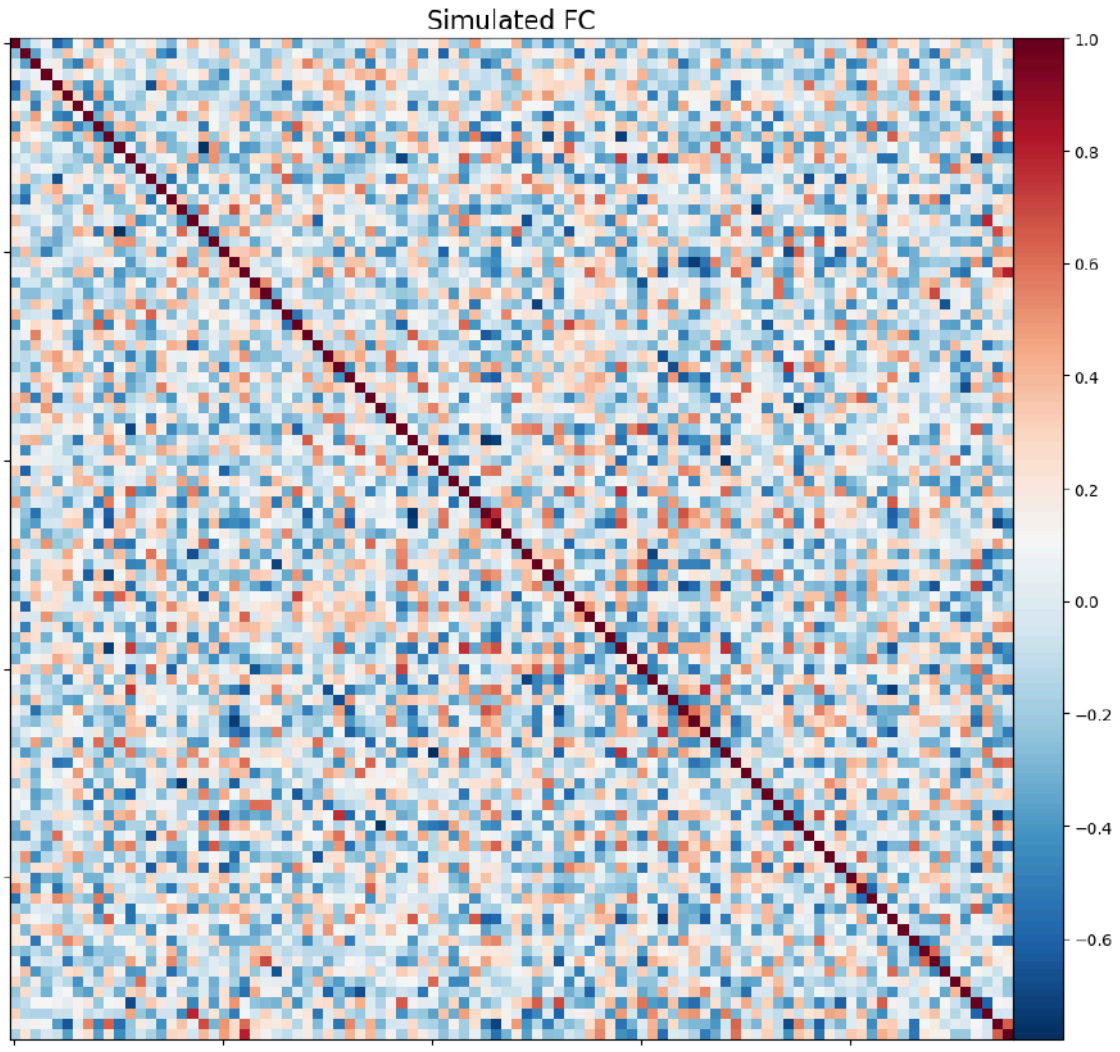

Fig 4.2.7.1: Simulated FC

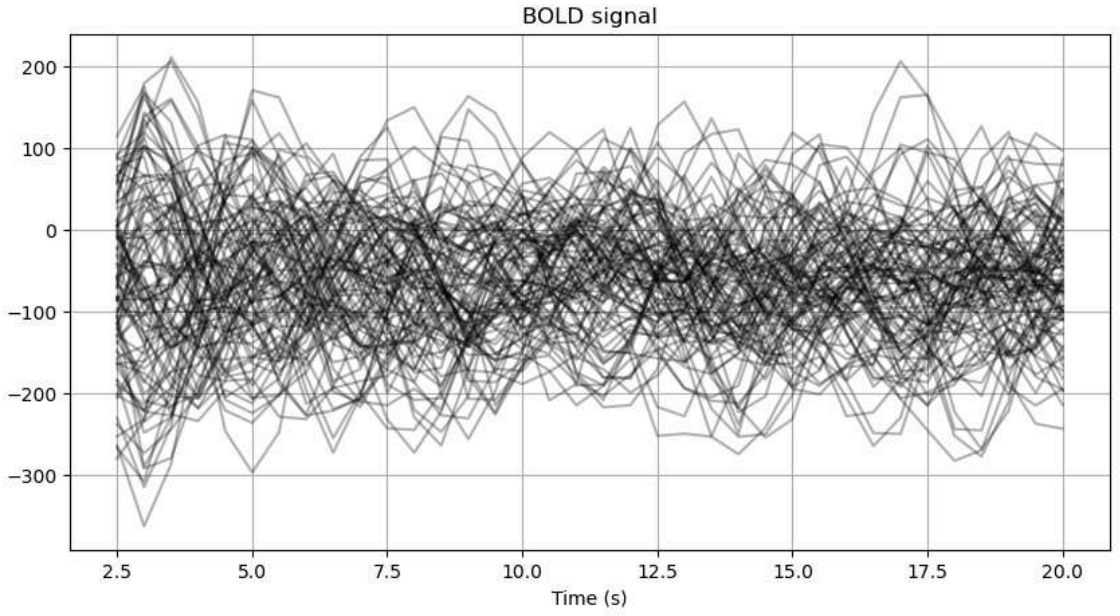

Fig 4.2.7.2: Simulated BOLD Time Series

4.2.8 Towards optimization

Optimization algorithms are diverse, each tailored to solve specific types of problems. We looked to optimize our simulation to better mimic empirical data. However, one common challenge faced by computational neuroscientists is the computational time and cost incurred when running a single simulation to completion. It thus makes traditional grid searches impractical. Bayesian optimization offers a solution to this problem by incorporating an informed hyperparameter search with a degree of randomness.

Bayesian optimization consists primarily of two functions:

1. Black box function f(x) - represents the objective to optimize
2. Acquisition function a(x)- guides the search for optimal parameters.

First, initial parameter values are randomly generated, and the corresponding function outputs are measured. Then, a Gaussian process model is trained using the observed data. The acquisition function utilizes this model to propose new parameter values for evaluation, aiming to maximize the expected improvement in function performance. This process iterates until a parameter value leading to the global optimum is found. Importantly, historical data is used to train the Gaussian process model at each iteration, enabling better predictions as more data becomes available. The Bayesian-Optimization package in Python [56] provides this complete functionality.

Given the large state-space of configurable parameters, it would not be feasible to optimize all the parameters of the simulation. After conducting numerous simulations manually, it became evident that only a select few parameters significantly influenced the resultant FC matrix. We thus decided to optimize the following parameters:

1. Sigmoidal Coupling
2. J- Average number of synapses between populations
3. Noise

In our study, the black box function carried out the simulation and returned the MSE between the simulated FC and empirical FC. Given the goal of Bayesian optimization is to maximize the value returned by the black box function, we thus returned the negative value of the MSE. The deployment of Bayesian Optimization facilitated a systematic exploration of the extensive hyperparameter space, capitalizing on prior evaluations to inform subsequent sampling decisions.

Results

The optimization process was executed across 100 iterations yielding a global minima of MSE as 0.094. After comparing the results of the simulation before and after optimization, there was a noticeable reduction of MSE by 48.2%, underscoring the efficacy of the Bayesian optimization process.

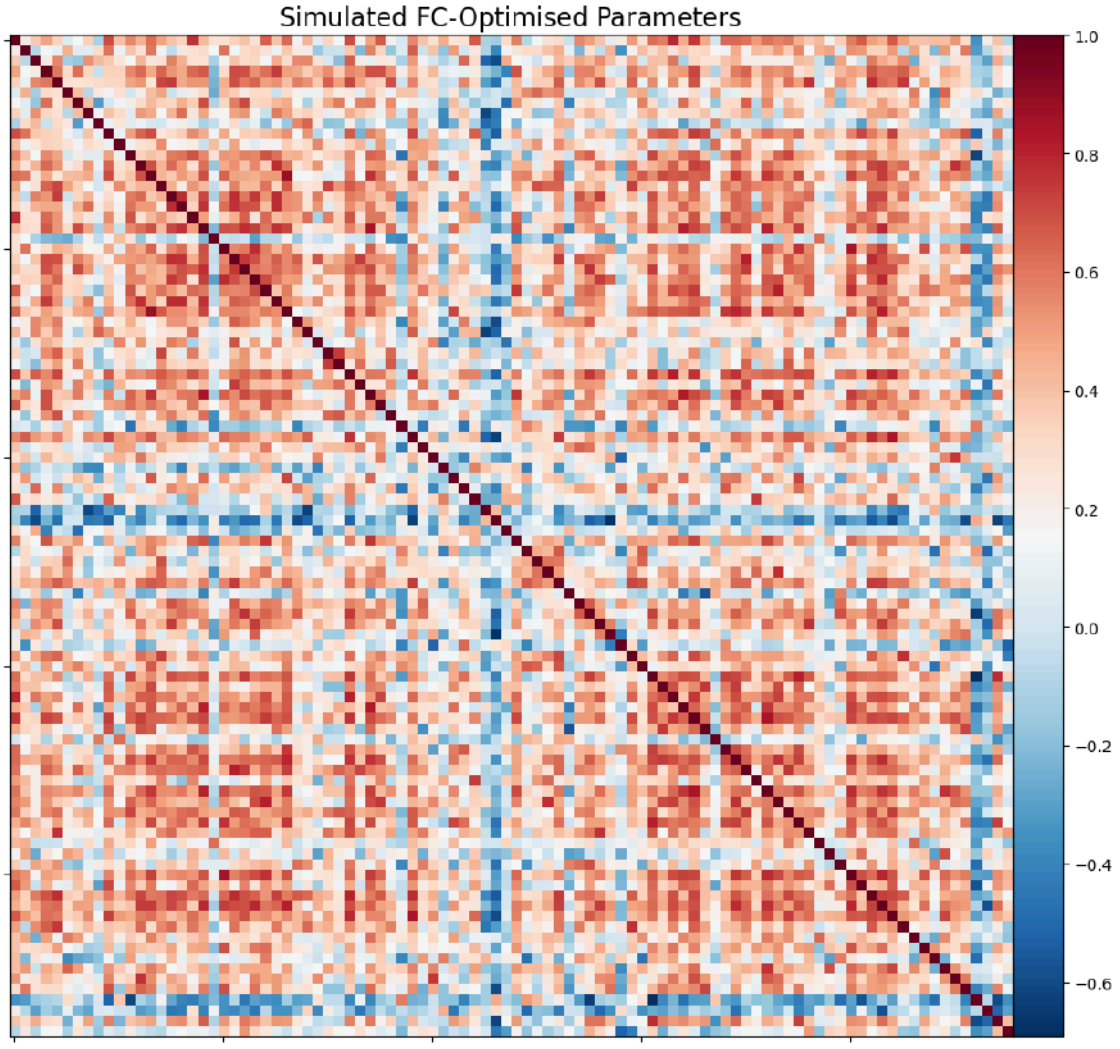

Fig 4.2.8.1: Simulated FC after optimization

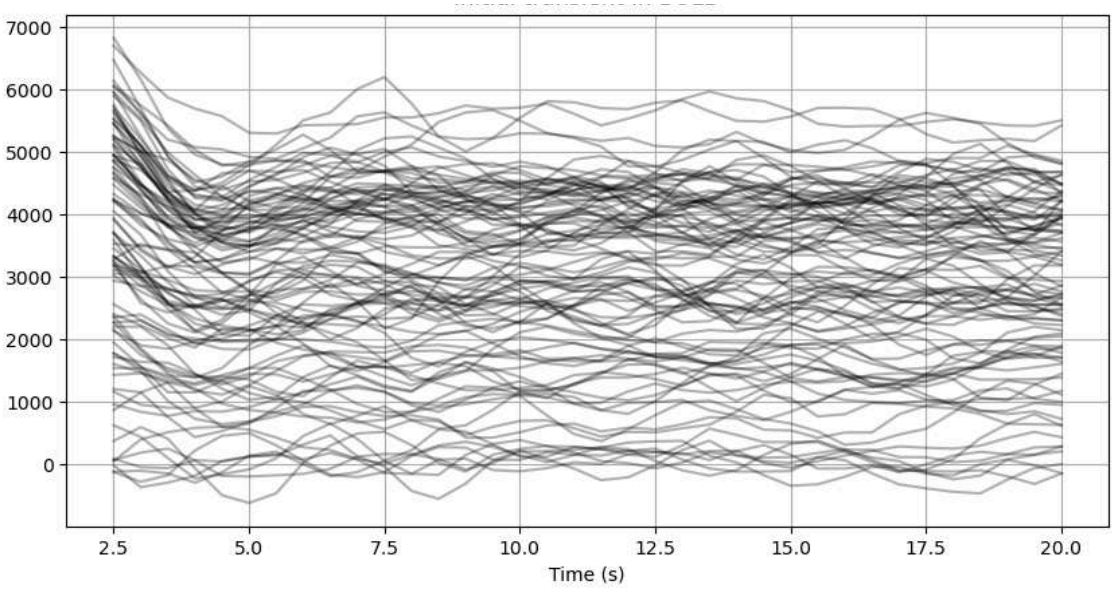

Fig 4.2.8.1: Simulated BOLD Time Series after optimization

CHAPTER 5:

TESTING AND VALIDATION

Processing empirical data

The dataset used for validation of the simulation, was the COBRE dataset [31] used previously for the validation of biomarkers. The COBRE dataset contained preprocessed fMRI images of patients and controls stored in the Neuroimaging Informatics Technology Initiative (NIfTI) format. We thus needed to generate FC matrices of each of these fMRI files. To this end, we first obtained the Connectivity-96 parcellation map [45] [54] along with the labels which would enable us to map the 96 regions on the fMRI. Subsequently, a masker is constructed using Nilearn to extract time series data from each fMRI file based on the parcellation and region labels on Connectivity-96. A correlation matrix i.e FC matrix is then computed based on the timeseries for each of the regions for the patients and controls.

In order to capture the dynamics across patients, a single FC matrix is computed for all patients by taking the mean across subjects shown in Fig 5.1(A) to capture the net effects. The same was also carried out for all the healthy controls illustrated in Fig 5.1(B) .

A) B)

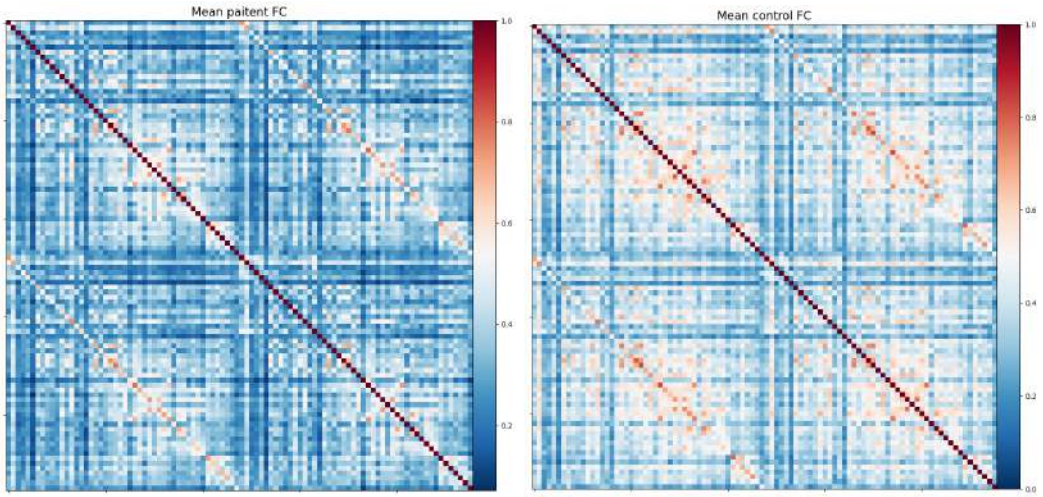

Fig 5.1: (A) Mean Patient FC and (B) Mean Control FC

Detecting Presence of Biomarkers

To assess the efficacy of our simulations, we looked to test the existence of biomarkers put forth by various studies. A pertinent impediment was the different regions that were specified in the biomarkers, some of which were not directly present among the 96 regions that our model simulated. This issue arises due to the different mappings/parcellations used by researchers. To mitigate this, we identified regions based on their proximal positions on anatomical maps and worked to find an analogous mapping to Connectivity-96.

Our approach is to compare for a given region/network, the simulated FC, representing a schizophrenia brain, to that of the healthy controls' FC. We then compare this against the experimental study (Section 2.3) i.e, whether FC increased or decreased in patients with schizophrenia as compared to healthy controls thus verifying the presence or absence of the biomarker within our simulation. Towards this, we initially designed Python-based functions to compute intra-region FC, intra-network FC, inter-region FC, and inter-network FC based on the regions/networks provided as input. For each biomarker, the appropriate computation was carried out on the simulated FC matrix as well the healthy controls' FC matrix. Finally, the two values were compared.. Table 5.1 shows the biomarker that was tested along with the result i.e whether the simulated FC indicated the presence of the biomarker.

Results

Biomarker	**Simulated FC**
Reduced ventral striatum-hippocampus coupling [3]	True
Reduced intra-striatal FC [1]	True
Decreased FC between the frontoparietal network and the visual networks [64]	False
Increased FC between the default mode network and the central executive networks [65]	True
Increased FC between the sensory processing and the default mode network [66]	True
Increase in FC within the default mode network [67]	True

Table 5.1: Test for presence of biomarkers for schizophrenia in the optimized simulation

CHAPTER 6:

CONCLUSION AND FUTURE SCOPE

Firstly, a thorough study on fMRI biomarkers for schizophrenia was successfully carried out. The study led to significant findings, notably emphasizing the striatal region of the brain as a focal point for these biomarkers. We successfully replicated Functional Striatal Abnormalities score biomarker on an independent dataset resulting in an accuracy exceeding 70%. Moreover, leveraging an SVM approach targeting the striatal region underscored the dysfunction associated with the striatum with an impressive classification accuracy of 84% between patients and controls. A large-scale brain simulation was carried out using The Virtual Brain console that incorporated region-level dysfunction informed by several studies on neural aberrations in the functional imaging of schizophrenia. A BOLD signal was simulated from which a Functional Connectivity Matrix was generated. The simulation's parameters such as coupling and noise were further improved by Bayesian optimization, using empirical data to inform the optimization. The optimization successfully reduced the Mean Squared Error between the simulated and empirical FC by 48%. Lastly we looked to verify the existence of biomarkers for schizophrenia. We successfully detected the presence of 5 out of 6 biomarkers that we reviewed, underscoring the success of the region-level tweaking of the simulation.

Our simulation was tailored to maintain similarity with data from multiple schizophrenia patients, rather than focusing solely on a single patient. While this approach allows us to capture the variability present across patient populations, it presents limitations for individualized applications. We suggest a shift towards individualized modeling, where models mimic the unique characteristics of a single patient's brain. This personalized approach provides a greater ability of the model to mimic the activity patterns of the patient's brain, enabling the identification of patient-specific biomarkers and treatment targets. In exploring the future scope of our project, it becomes evident that large-scale simulations, while valuable in elucidating broad neural dynamics, may fall short in capturing the nuanced aberrations present at the neuron or even cellular level. In this regard, embracing a multiscale perspective appears to be the way forward. By integrating data and insights across various levels of neural organization, from molecular and cellular mechanisms to whole-brain dynamics, multiscale modeling would seem to offer a more comprehensive understanding of schizophrenia pathology. However the primary impediment to multi-scale simulation is the enormous compute power required. Therefore there is a need for several advances in code optimization, parallelisation and processes of the like to be developed and studied to be performed when dealing with such complexities.

References

[1] A. Li, A. Zalesky, W. Yue, et al., “A neuroimaging biomarker for striatal dysfunction in schizophrenia”, Nature Medicine, vol. 26, no. 4, pp. 558–565, 2020

[2] D. K. Sarpal, M. Argyelan, D. G. Robinson,et al. “Baseline striatal functional connectivity as a predictor of response to antipsychotic drug treatment”,American Journal of Psychiatry, vol. 173, no. 1, pp. 69–77,2016

[3] K. Schwarz, C. Moessnang, J. I. Schweiger, et al., “Ventral striatal–hippocampus coupling during reward processing as a stratification biomarker for psychotic disorders”, Biological Psychiatry, vol. 91, no. 2,pp. 216–225, 2022.

[4] D. Shi, H. Zhang, G. Wang, et al., “Neuroimaging biomarkers for detecting schizophrenia: A resting-state functional mri-based radiomics analysis”, Heliyon, vol. 8, no. 12, e12276, 2022, issn: 2405-8440. doi: https : / / doi . org / 10 . 1016 / j . heliyon . 2022 . e12276. [Online].Available: https:// www . sciencedirect . com / science / article /pii/S2405844022035642.

[5] B. Cao, R. Y. Cho, D. Chen, et al., “Treatment response prediction and individualized identification of first-episode drug-naive schizophrenia using brain functional connectivity”, Molecular psychiatry, vol. 25, no. 4, pp. 906–913, 2020.

[6] L.- B. Cui, M. Cai, X.-R. Wang, et al., “Prediction of early response to overall treatment for schizophrenia: A functional magnetic resonance imaging study”, Brain and Behavior, vol. 9, no. 2, e01211, 2019.

[7] J. Gao, R. Jiang, X. Tang, et al., “A neuromarker for deficit syndrome in schizophrenia from a combination of structural and functional magnetic resonance imaging”, CNS Neuroscience & Therapeutics, 2023.

[8] R. Jing, P. Li, Z. Ding, et al., “Machine learning identifies unaffected first-degree relatives with functional network patterns and cognitive impairment similar to those of schizophrenia patients”, Human brain mapping, vol. 40, no. 13, pp. 3930–3939, 2019.22

[9] N. Koutsouleris, E. M. Meisenzahl, C. Davatzikos, et al., “Use of neuroanatomical pattern classification to identify subjects in at-risk mental states of psychosis and predict disease transition”, Archives of general psychiatry, vol. 66, no. 7, pp. 700–712, 2009.

[10] B. Yao, S. F. Neggers, R. S. Kahn, and K. N. Thakkar, “Altered thalamocortical structural connectivity in persons with schizophrenia and healthy siblings”, NeuroImage: Clinical, vol. 28, p. 102 370, 2020.

[11] Brain, V. (n.d.). *The virtual brain*. The Virtual Brain. https://www.thevirtualbrain.org/tvb/

[12] Michael Schirner, Simon Rothmeier, Viktor K. Jirsa, Anthony Randal McIntosh, Petra Ritter, An automated pipeline for constructing personalized virtual brains from multimodal neuroimaging data, NeuroImage, Volume 117, 2015, Pages 343-357, ISSN 1053-8119, https://doi.org/10.1016/j.neuroimage.2015.03.055.

[13] Team, B. (2020, January 17). The Brian Simulator. The Brian Spiking Neural Network Simulator. https://briansimulator.org/

[14] NEST Simulator. (n.d.). https://www.nest-simulator.org/

[15] What is NEURON? | NEURON. (n.d.). https://www.neuron.yale.edu/neuron/what_is_neuron

[16] The GENESIS simulator. (n.d.). http://genesis-sim.org/

[17] Park, B., Byeon, K., & Park, H. (2019). FUNP (Fusion of Neuroimaging Preprocessing) Pipelines: a fully automated preprocessing software for functional magnetic resonance imaging. *Frontiers in Neuroinformatics*, *13*. https://doi.org/10.3389/fninf.2019.00005

[18] Resample an image to a template. (n.d.). Nilearn. https://nilearn.github.io/stable/auto_examples/06_manipulating_images/plot_resample_to_template.html

[19] Smoothing an image. (n.d.). Nilearn. https://nilearn.github.io/stable/auto_examples/06_manipulating_images/plot_smooth_mean_image.html#smoothing-an-image

[20] Hashimoto, Y., Ogata, Y., Honda, M., & Yamashita, Y. (2021). Deep Feature Extraction for Resting-State Functional MRI by Self-Supervised Learning and Application to Schizophrenia Diagnosis. *Frontiers in neuroscience*, 15, 696853. https://doi.org/10.3389/fnins.2021.696853

[21] Orrù, G., Pettersson-Yeo, W., Marquand, A. F., Sartori, G., & Mechelli, A. (2012). Using Support Vector Machine to identify imaging biomarkers of neurological and psychiatric disease: A critical review. *Neuroscience & Biobehavioral Reviews*, *36*(4), 1140–1152. https://doi.org/10.1016/j.neubiorev.2012.01.004

[22] Anaconda Navigator — Anaconda documentation. (n.d.). https://docs.anaconda.com/free/navigator/index.html

[23] Project Jupyter Documentation — Jupyter Documentation 4.1.1 alpha documentation. (n.d.). https://docs.jupyter.org/en/latest/

[24] Google Colab. (n.d.). *Notebooks – Colab.Google*. colab.google. https://colab.google/notebooks/

[25] *Welcome to Python.org*. (n.d.). Python.org. https://www.python.org/doc/

[26] *Nilearn*. (n.d.). Nilearn. https://nilearn.github.io/stable/index.html

[27] scikit-learn: machine learning in Python — scikit-learn 1.4.2 documentation. (n.d.-b). https://scikit-learn.org/stable/

[28] S. Wang, Y. Zhang, L. Lv, et al., "Abnormal regional homogeneity as a potential imaging biomarker for adolescent-onset schizophrenia: A resting-state fmri study and support vector machine analysis",Schizophrenia research, vol. 192, pp. 179–184, 2018.

[29] Debo Dong, Mingjun Duan, Yulin Wang, Xingxing Zhang, Xiaoyan Jia, Yingjia Li, Fei Xin, Dezhong Yao, Cheng Luo, Reconfiguration of Dynamic Functional Connectivity in Sensory and Perceptual System in Schizophrenia, Cerebral Cortex, Volume 29, Issue 8, August 2019, Pages 3577–3589.

[30] Zhou, Y., Shu, N., Liu, Y., Song, M., Hao, Y., Liu, H., Yu, C., Liu, Z., & Jiang, T. (2008). Altered resting-state functional connectivity and anatomical connectivity of hippocampus in schizophrenia. Schizophrenia research, 100(1-3), 120–132. https://doi.org/10.1016/j.schres.2007.11.039

[31] Bellec, P. (2016). COBRE preprocessed with NIAK 0.17-lightweight release. https://doi.org/10.6084/m9.figshare.4197885.v1

[32] Zhao, Y., Li, X., Zhang, W., Zhao, S., Makkie, M., Zhang, M., ... & Liu, T. (2018). Modeling 4D fMRI data via spatio-temporal convolutional neural networks (ST-CNN). In *Medical Image Computing and Computer Assisted Intervention–MICCAI 2018: 21st International Conference, Granada, Spain, September 16-20, 2018, Proceedings, Part III 11* (pp. 181-189). Springer International Publishing.

[33] Sanz Leon, P., Knock, S. A., Woodman, M. M., Domide, L., Mersmann, J., McIntosh, A. R., & Jirsa, V. (2013). The Virtual Brain: A simulator of primate brain network dynamics. *Frontiers in Neuroinformatics*, *7*, 47900. https://doi.org/10.3389/fninf.2013.00010

[34] Schirner, M., Domide, L., Perdikis, D., Triebkorn, P., Stefanovski, L., Pai, R., Prodan, P., Valean, B., Palmer, J., Langford, C., Blickensdörfer, A., Van der Vlag, M., Diaz-Pier, S., Peyser, A., Klijn, W., Pleiter, D., Nahm, A., Schmid, O., Woodman, M., ... Ritter, P. (2022). Brain simulation as a cloud service: The Virtual Brain on EBRAINS. NeuroImage, 251, 118973. https://doi.org/10.1016/j.neuroimage.2022.118973

[35] nilearn.masking.apply_mask. (n.d.). Nilearn. https://nilearn.github.io/dev/modules/generated/nilearn.masking.apply_mask.html

[36] Console Interfaces of TheVirtualBrain: https://docs.thevirtualbrain.org/manuals/UserGuide/UserGuide-Shell.html

[37] Moran, L. V., Tagamets, M. A., Sampath, H., O'Donnell, A., Stein, E. A., Kochunov, P., & Hong, L. E. (2013). Disruption of Anterior Insula Modulation of

Large-Scale Brain Networks in Schizophrenia. *Biological Psychiatry*, *74*(6), 467-474. https://doi.org/10.1016/j.biopsych.2013.02.029

[38] Lynall, M.-E., Bassett, D. S., Kerwin, R., McKenna, P. J., Kitzbichler, M., Muller, U., & Bullmore, E. (2010). Functional Connectivity and Brain Networks in Schizophrenia. Journal of Neuroscience, 30(28), 9477–9487. https://doi.org/10.1523/JNEUROSCI.0333-10.2010

[39] Shen, L., Tsai, J., Lin, P., & Yang, A. C. (2023). Progressive brain abnormalities in schizophrenia across different illness periods: A structural and functional MRI study. *Schizophrenia*, *9*(1). https://doi.org/10.1038/s41537-022-00328-7

[40] Jansen, B. H., & Rit, V. G. (1995). Electroencephalogram and visual evoked potential generation in a mathematical model of coupled cortical columns. Biological cybernetics, 73(4), 357-366.

[41] Cakan, C., Jajcay, N., & Obermayer, K. (2021). neurolib: A Simulation Framework for Whole-Brain Neural Mass Modeling. Cognitive Computation, 15(4), 1132–1152. https://doi.org/10.1007/s12559-021-09931-9

[42] Extracting signals from a brain parcellation. (n.d.). Nilearn. https://nilearn.github.io/dev/auto_examples/03_connectivity/plot_signal_extraction.html

[43] Jansen-Rit on the whole brain scale. (n.d.). Google Groups. https://groups.google.com/g/tvb-users/c/Tv9qDoBsJsI/m/gHVym-7TAAAJ

[44] Shen, K., Bezgin, G., Schirner, M. et al. A macaque connectome for large-scale network simulations in TheVirtualBrain. Sci Data 6, 123 (2019). https://doi.org/10.1038/s41597-019-0129-z

[45] Bezgin G, Solodkin A, Bakker R, Ritter P, McIntosh AR (2017) Mapping complementary features of cross-species structural connectivity to construct realistic "Virtual Brains". Human Brain Mapping, 38: 2080-2093. doi: 10.1002/hbm.23506

[46] Sharma, A. (2018, November 3). Algorithms for hyperparameter optimization in Python. *Medium*. https://towardsdatascience.com/algorithms-for-hyperparameter-optimization-in-python-edda4bdb167

[47] The role of inhibition in resting-state fMRI negative correlations Shreyas Harita, Davide Momi, Zheng Wang, Sorenza P. Bastiaens, John D. Griffiths bioRxiv 2024.03.01.583030; doi: https://doi.org/10.1101/2024.03.01.583030

[48] Buxton RB, Frank LR. A Model for the Coupling between Cerebral Blood Flow and Oxygen Metabolism during Neural Stimulation. Journal of Cerebral Blood Flow & Metabolism. 1997;17(1):64-72. doi:10.1097/00004647-199701000-00009

[49] Friston, K. J., Mechelli, A., Turner, R., & Price, C. J. (2000). Nonlinear responses in fMRI: the Balloon model, Volterra kernels, and other hemodynamics. NeuroImage, 12(4), 466–477. https://doi.org/10.1006/nimg.2000.0630

[50] HRF Kernel Equation — TVB 2.9-18157 documentation. (n.d.). https://docs.thevirtualbrain.org/api/tvb.datatypes.html#traited-class-tvb-datatypes-equations-firstordervolterra

[51] Additive Noise- Stochastic Integration in TVB https://docs.thevirtualbrain.org/api/tvb.simulator.noise.html#traited-class-tvb-simulator-noise-additive

[52] Shahhosseini Y, Miranda MF. Functional Connectivity Methods and Their Applications in fMRI Data. Entropy (Basel). 2022 Mar 11;24(3):390. doi: 10.3390/e24030390. PMID: 35327901; PMCID: PMC8946919.

[53] Pearson Correlation Coefficent in Numpy https://numpy.org/doc/stable/reference/generated/numpy.corrcoef.html

[54] The Regional-Map 96 (RM96) parcellation- Github https://github.com/McIntosh-Lab/tvb-ukbb/tree/main/templates/parcellations/RM96

[55] Jansen, B. H., & Rit, V. G. (1995). Electroencephalogram and visual evoked potential generation in a mathematical model of coupled cortical columns. Biological cybernetics, 73(4), 357-366.

[56] Bayesian Optimisation- Python Package- https://bayesian-optimization.github.io/BayesianOptimization/index.html#

[57] Masking data: from 4D Nifti images to 2D data arrays- Nilearn https://nilearn.github.io/dev/manipulating_images/manipulating_images.html#masking-data-from-4d-nifti-images-to-2d-data-arrays

[58] Brant-stable/template at master · YongLiuLab/brant-stable — github.com, https://github.com/YongLiuLab/brant- stable/tree/master/ template/.

[59] Wang, S., Rao, B., Chen, L., Chen, Z., Fang, P., Miao, G., ... & Liao, W. (2021). Using fractional amplitude of low-frequency fluctuations and functional connectivity in patients with post-stroke cognitive impairment for a simulated stimulation program. Frontiers in Aging Neuroscience, 13, 724267.

[60] Rao, C., & Liu, Y. (2020). Three-dimensional convolutional neural network (3D-CNN) for heterogeneous material homogenization. Computational Materials Science, 184, 109850.

[61] Matplotlib — Visualization with Python. (n.d.). https://matplotlib.org/

[62] Tran The, J., Ansermet, J. P., Magistretti, P. J., & Ansermet, F. (2022). Hyperactivity of the default mode network in schizophrenia and free energy: A dialogue between Freudian theory of psychosis and neuroscience. Frontiers in Human Neuroscience, 16, 956831.

[63] Zhang, F., Hua, B., Wang, M. et al. Regional homogeneity abnormalities of resting state brain activities in children with growth hormone deficiency. Sci Rep 11, 334 (2021). https://doi.org/10.1038/s41598-020-79475-9

[64] Jiang L, Zuo XN. Regional Homogeneity: A Multimodal, Multiscale Neuroimaging Marker of the Human Connectome. Neuroscientist. 2016 Oct;22(5):486-505. doi: 10.1177/1073858415595004. Epub 2015 Jul 13. PMID: 26170004; PMCID: PMC5021216.

[65] Manoliu A., Riedl V., Zherdin A., Mühlau M., Schwerthöffer D., Scherr M., et al. (2014). Aberrant dependence of default mode/central executive network interactions on anterior insular salience network activity in schizophrenia. Schizophrenia Bulletin, 40(2), 428–437. [DOI: 10.1093/schbul/sbt037]

[66] Tu P. C., Lee Y. C., Chen Y. S., Li C. T., Su T. P. (2013). Schizophrenia and the brain's control network: Aberrant within- and between-network connectivity of the frontoparietal network in schizophrenia. Schizophrenia Research, 147(2–3), 339–347. [DOI: 10.1016/j.schres.2013.04.011]

[67] LHu ML, Zong XF, Mann JJ, Zheng JJ, Liao YH, Li ZC, He Y, Chen XG, Tang JS. A Review of the Functional and Anatomical default mode network in Schizophrenia. Neurosci Bull. 2017 Feb;33(1):73-84. doi: 10.1007/s12264-016-0090-1. Epub 2016 Dec 19. PMID: 27995564; PMCID: PMC5567552.

[68] Small-world indices via network efficiency for brain networks from diffusion MRI - Scientific Figure on ResearchGate. Available from: https://www.researchgate.net/figure/Five-parcellation-atlases-For-their-identification-see-the-Brain-parcellation-section_fig2_326231084 [accessed 10 May, 2024]

[69] Personalization of hybrid brain models from neuroimaging and electrophysiology data - Scientific Figure on ResearchGate. Available from: https://www.researchgate.net/figure/Figure-A1-Diagram-of-Jansen-and-Rit-model-for-a-cortical-column-Each-color-and-shape_fig4_328734658 [accessed 10 May, 2024]

[70] Zhuo, C., Wang, C., Wang, L. et al. Altered resting-state functional connectivity of the cerebellum in schizophrenia. Brain Imaging and Behavior 12, 383–389 (2018). https://doi.org/10.1007/s11682-017-9704-0

[71] Fan L, Li H, Zhuo J, Zhang Y, Wang J, Chen L, Yang Z, Chu C, Xie S, Laird AR, Fox PT, Eickhoff SB, Yu C, Jiang T. The Human Brainnetome Atlas: A New Brain Atlas Based on Connectional Architecture. Cereb Cortex. 2016 Aug;26(8):3508-26.

doi: 10.1093/cercor/bhw157. Epub 2016 May 26. PMID: 27230218; PMCID: PMC4961028.

[72] TVB- Jansen Rit Model parameters and definitions https://docs.thevirtualbrain.org/_modules/tvb/simulator/models/jansen_rit.html

[73] TVB- Sigmoidal Jansen-Rit Coupling Scheme https://docs.thevirtualbrain.org/api/tvb.simulator.coupling.html#traited-class-tvb-simulator-coupling-sigmoidaljansenrit